Astrometric effects of gravitational wave backgrounds with non-Einsteinian polarizations

Deyan P. Mihaylov,[1,*] Christopher J. Moore,[2,3,†] Jonathan R. Gair,[4,‡]
Anthony Lasenby,[5,6,§] and Gerard Gilmore[1,‖]

[1]*Institute of Astronomy, University of Cambridge, Madingley Road, Cambridge,*
CB3 0HA, United Kingdom
[2]*Centro de Astrofísica e Gravitação – CENTRA, Departamento de Física, Instituto Superior Técnico – IST,*
Universidade de Lisboa – UL, Av. Rovisco Pais 1, 1049-001 Lisboa, Portugal
[3]*DAMTP, Centre for Mathematical Sciences, University of Cambridge, Wilberforce Road,*
Cambridge, CB3 0WA, United Kingdom
[4]*School of Mathematics, University of Edinburgh, Peter Guthrie Tait Road, Edinburgh,*
EH9 3FD, United Kingdom
[5]*Astrophysics Group, Cavendish Laboratory, J J Thomson Avenue, Cambridge CB3 0HE, United Kingdom*
[6]*Kavli Institute for Cosmology, Madingley Road, Cambridge CB3 0HA, United Kingdom*

The Gaia mission offers a new opportunity to search for the low-frequency gravitational wave background using astrometric measurements. In this paper, the astrometric effect of gravitational waves is reviewed, with a particular focus on the effect of non-Einsteinian gravitational wave polarizations. A stochastic gravitational wave background generates a correlated vector field of astrometric deflections on the sky. A convenient decomposition for the correlation matrix is introduced, enabling it to be calculated for all possible gravitational wave polarizations and compared to the redshift correlations from the pulsar-timing literature; in the case of a general relativity background of transverse traceless gravitational waves, this also allows us to identify an astrometric analog of the famous Hellings-Downs curve. Finally, the cross correlation between the redshift and astrometric signal is also calculated; this may form the basis for future joint pulsar-timing and astrometry searches for arbitrarily polarized gravitational wave backgrounds.

I. INTRODUCTION

The first direct detection of gravitational waves (GWs) from a binary black hole was achieved in September 2015 by the LVC Collaboration using the ground-based Advanced LIGO detectors [1]. This event, as well as subsequent binary black hole detections [2–5], and the first multimessenger observations of a binary neutron star merger [6], have paved the way for the development of a host of new research topics in astronomy, astrophysics and cosmology [7–10]. In particular, gravitational waves afford the possibility to test the theory of general relativity (GR) in regimes which are inaccessible through light-based observations (e.g., strong gravity), and to constrain the deviations from general relativity far better than has previously been possible [11–13].

There are, however, GW tests of GR which are difficult or impossible to perform with current instruments. For example,

the geometry of the two LIGO detectors alone hinders accurate determination of the GW polarization; this has been improved by the addition of Virgo which helped constrain the polarization content of GW170814 [4]. However, there may still exist combinations of GW polarizations (the transverse and longitudinal scalar modes) which laser interferometers cannot distinguish [14,15]. It is well known that pulsar timing arrays (PTAs) provide one method which can distinguish between all six possible GW polarizations [16] and can even have an enhanced response to some non-Einsteinian polarizations [17]. In this paper another technique capable of distinguishing the six GW polarizations is considered.

The Gaia mission, launched in 2013 by ESA, is carrying out a thorough mapping of more than a billion objects in the Milky Way [18]. As part of this survey, star positions, velocities, and accelerations (among other observables) will be mapped with an unprecedented precision; this new map of the Milky Way objects will allow for an entirely updated understanding of the dynamics and composition of our Galaxy and of the Local Group [19].

The idea of using high-precision astrometric measurements as an alternative avenue to detecting gravitational

[*]d.mihaylov@ast.cam.ac.uk
[†]cjm96@cam.ac.uk
[‡]j.gair@ed.ac.uk
[§]a.n.lasenby@mrao.cam.ac.uk
[‖]gil@ast.cam.ac.uk

wave signals is not new: the authors of Ref. [20] were the first to examine the physical principles at play, and later the authors of Ref. [21] applied them to quasar proper motions. More recently the authors of Ref. [22] published an in-depth analysis of the concept applied to astrometric measurements, the authors of Ref. [23] evaluated the viability of finding this effect in detector data, and the authors of Ref. [24] discussed it in direct relation to the Gaia mission. The approach has been investigated numerically in the context of Gaia, and future data releases promise better sensitivity to single GW sources than existing techniques in a certain frequency range [25]. This article explores the possibility of using such high-precision astrometric measurements to ascertain the polarization of a stochastic GW background, and hence constrain modified theories of gravity.

Within GR, gravitational waves travel at the speed of light and carry a superposition of two transverse, traceless polarization modes, usually denoted $+$ and $\times$ [26]. Generic metric theories of gravity have up to four additional polarization modes: a purely transverse scalar mode, two vectorial modes with mixed transverse and longitudinal properties, and a purely longitudinal scalar mode [15]. It should be noted that modified theories of gravity must now satisfy the polarization constraints from the LIGO-Virgo observations (e.g., Ref. [4]) of compact binary sources in the frequency range $\sim 10^1$–10^3 Hz. In general, these polarization modes may travel at speeds other than the speed of light; however this is strongly constrained by the recent electromagnetic and GW multimessenger observations [13]. Detections of GWs using astrometric methods would allow for additional constraints to be placed on their polarization and speed. This paper considers all six GW polarizations, but the discussion is restricted to waves traveling at the speed of light.

While still not explicitly detected, another possible target for gravitational wave detectors is a stochastic gravitational wave background created by a large number of random, uncorrelated, and individually unresolvable sources. According to their origin, backgrounds can be classed as astrophysical or cosmological. Astrophysical sources range from supernovae and mergers of compact objects (black hole–black hole, black hole–neutron star, and neutron star–neutron star binaries) to supermassive black hole binaries. Backgrounds of this origin are generally believed to have a power-law spectrum and exist at frequencies above $\sim 10^{-12}$ Hz [27]. Cosmological backgrounds, on the other hand, include early-Universe events like reheating or inflation, or even more exotic alternatives like primordial black hole mergers or QCD phase transitions. These generally have more unusual spectra, and are more powerful at lower frequencies than astrophysical backgrounds. Astrophysical backgrounds, specifically supermassive black hole binaries corresponding to galaxy mergers, are by far the most promising in the context of astrometric and

PTA-based methods for detection. The most constraining upper limits on the stochastic GW background at frequencies of several nanohertz come from pulsar timing. The North American Nanohertz Observatory for Gravitational Waves [28] and the European Pulsar Timing Array [29] placed 95% Bayesian upper limits on the amplitude of a stochastic gravitational wave background of 1.5×10^{-4} and 3.0×10^{-15} respectively at a frequency of 1 year^{-1}. Currently the most stringent limit comes from the Parkes Pulsar Timing Array which placed a 95% upper limit on the amplitude of 1.0×10^{-15} at a frequency of 1 year^{-1} [30] while the International Pulsar Timing Array [31] has placed a 2σ upper limit of 1.7×10^{-15} at the same frequency.

This article analyses the astrometric response to a gravitational wave and the detector cross-correlation functions (or overlap reduction functions) for an astrophysical background in the context of all possible gravitational wave polarization states. In Sec. II the relativistic principles that are responsible for the periodic shift in a star's apparent position on the sky due to a gravitational wave are presented. Similar analyses have been published previously (e.g., Ref. [22]), but it is repeated here with a focus on the astrometric response to non-GR polarization states. Section III summarizes the mathematical formulation of GW polarization tensors. The characteristic astrometric patterns produced by each polarization are then plotted and analyzed in terms of the geometry of the astrometric response function. The expected value of the correlation between the response function of two independent detectors is defined and derived for each of the polarization states in Sec. IV. Their significance and possible applications are also presented, alongside suitable depictions of their geometry. Pulsar timing and astrometry are two techniques which are capable of detecting GWs from similar sources. It is therefore interesting to consider the possibility of combining PTA and astrometric data sets to achieve improved sensitivities. As a first step in this direction, Sec. V considers the cross correlation between the astrometric deflection and the PTA measured redshift for each of the possible GW polarizations.

After this paper was submitted a preprint appeared [32] which had independently obtained similar results for the astrometric correlation functions presented in Sec. IV of this paper. After accounting for somewhat different notation, their results agree with those presented here. Reference [32] does not present the redshift-astrometry correlations described in Sec. V of this paper, but they do present results for the correlation coefficients of a vector spherical harmonic representation of the astrometric response. This is written in terms of an angular power spectra function, and is not computed here.

The astrometric correlations due to a stochastic background of GWs with non-Einsteinian polarizations have not been explored previously. However, the redshift correlations due to such backgrounds have been explored

previously, in the context of pulsar timing arrays. Notably, Ref. [16] set out a thorough overview of the topic, and [33] calculated all relevant correlations for scalar and vector backgrounds. Throughout this paper, the astrometric correlations derived will be compared with the existing results for the redshift correlations.

II. ASTROMETRIC RESPONSE TO A GRAVITATIONAL WAVE

Astrometric measurements of any distant objects could, in principle, be used to detect GWs (the term "star" will be used to refer to any such distant object, although the same reasoning applies to any light source). The telescope used for the astrometric measurements will not be at rest (Gaia orbits at the Sun-Earth L2 point, and moves on a Lissajous-type orbit) and it will be necessary to correct for the detector motion; the term "Earth" will be used to refer to the location of an idealized stationary observer, and for simplicity it will be assumed that the necessary corrections in the data have already been made. Figure 1 depicts the relationship between the "star," the gravitational wave source, and the "Earth."

In this section the periodic astrometric deflection of a distant "star" as viewed from the "Earth" due to a weak, plane-fronted GW signal is derived. The background space-time is assumed to be flat [the mostly positive metric $\eta_{\mu\nu} = \text{diag}(-, +, +, +)$ is used here] and only leading-order terms in the metric perturbation are retained. We designate coordinates in which the Earth is at the spatial origin, $x_E^\mu(t) = (t, 0)$, and the Star is at fixed spatial position, $x_S^\mu(t) = (t, x_S^i)$, with $x_S^i \equiv \text{const}$. While the results in this section are not new (in particular our derivation is similar to that in Ref. [22]) it will be useful to rederive them here, paying special attention to the case of non-Einsteinian polarization states. The reader might be interested to consult
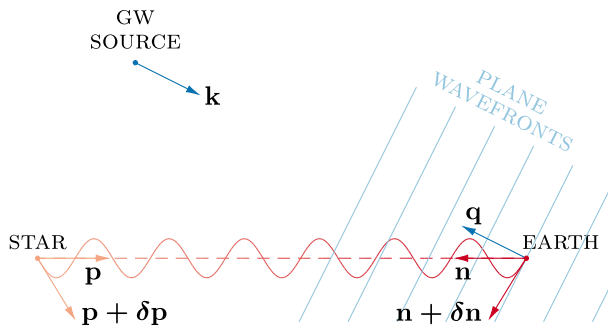

FIG. 1. An illustration of the geometric setup under consideration. The star lies on the past light cone of the Earth, and the two are linked by an unperturbed null geodesic with tangent vector p^μ and the apparent position of the star is given by $n_{\hat{i}}$. When the metric is perturbed by a GW with wave vector $k^\mu = -q^\mu$, the tangent to the null geodesic is perturbed, $p^\mu + \delta p^\mu$, along with the apparent position of the star, $n_{\hat{i}} + \delta n_{\hat{i}}$. The apparent position of the GW source is $q_{\hat{i}}$.

Ref. [34] for a simplified discussion of this effect and a comparison of the interferometric, pulsar timing, and astrometric methods for GW detection.

In the absence of a metric perturbation the star and the Earth are joined by the following one-parameter family of null geodesics in the flat space-time, labeled by t_0,

$$x_{t_0}^\mu(\lambda) = (\Omega\lambda + t_0, -\Omega\lambda n^i). \tag{1}$$

Here Ω is the unperturbed frequency of the photons coming from the star, $-n^i$ is a unit 3-vector in the direction of its propagation, the affine parameter λ varies from $\lambda_S \equiv -|\mathbf{x}_S|/\Omega$ to 0 between the star and the observer, and the tangent vector (4-momentum) $p^\mu \equiv dx^\mu/d\lambda = \Omega(1, -n^i)$ is null.

The observer (source) is equipped with a time-independent orthonormal tetrad $\epsilon_{\hat{a}}^\mu$ ($\sigma_{\hat{a}}^\mu$), satisfying $\eta_{\mu\nu}\epsilon_{\hat{a}}^\mu\epsilon_{\hat{b}}^\nu = \eta_{\mu\nu}\sigma_{\hat{a}}^\mu\sigma_{\hat{b}}^\nu = \eta_{\hat{a}\hat{b}}$, where the time-like basis vector is taken to be the 4-velocity, $\epsilon_{\hat{0}}^\mu = \sigma_{\hat{0}}^\mu = (1, 0, 0, 0)$. The tetrad is parallel transported along the worldline of the observer (source), who measures the following tetrad components (denoted with a hat) of the 4-momentum:

$$p_{\hat{a}} = \eta_{\mu\nu}p^\mu\epsilon_{\hat{a}}^\nu = -\Omega(1, n_{\hat{i}}), \quad \text{where } n_{\hat{i}} \equiv \epsilon_{\hat{i}}^\mu n_\mu \tag{2}$$

(and similarly for the source). The observed frequency is given by $\Omega_{\text{obs}} \equiv -p_{\hat{0}}$ while the astrometric position is given by $n_{\hat{i}} \equiv p_{\hat{i}}/p_{\hat{0}}$.

Now consider perturbing this setup with a monochromatic, plane-fronted GW with angular frequency ω radiated from a distant source in the direction of the vector q^i, extending over a region including the source and the observer (Fig. 1). The metric perturbation is given by

$$h_{\mu\nu}(t, x^i) = \Re\{H_{\mu\nu}\exp(ik_\rho x^\rho)\}, \tag{3}$$

where the $H_{\mu\nu}$ are small complex constants satisfying $H_{\mu\nu} = H_{\nu\mu}$, and the GW wave vector is $k^\mu = (\omega, -\omega q^i)$, where q^i is a 3-vector pointing from the Earth to the GW source. Hereafter, the $\Re$ is implicit in all complex expressions. Additionally, diffeomorphism invariance allows a spatial gauge choice to be made for the metric perturbation, $H_{0\mu} = 0$. In GR it is possible to further restrict to the well-known "transverse-traceless" gauge; this is not done here as our focus will be on alternative polarizations. The perturbed space-time is $g_{\mu\nu} = \eta_{\mu\nu} + h_{\mu\nu}$, and its inverse is $g^{\mu\nu} = \eta^{\mu\nu} - h^{\mu\nu}$. The connection coefficients for this metric are

$$\Gamma_{\nu\rho}^\mu = \frac{1}{2}g^{\mu\sigma}(\partial_\nu g_{\sigma\rho} + \partial_\rho g_{\nu\sigma} - \partial_\sigma g_{\mu\nu})$$
$$= \frac{1}{2}(\partial_\nu h^\mu{}_\rho + \partial_\rho h_\nu{}^\mu - \partial^\mu h_{\nu\rho}) + \mathcal{O}(h^2), \tag{4}$$

and the nonzero components are given explicitly by

$$\Gamma^0_{ij} = \frac{1}{2}\partial_0 h_{ij}, \qquad \Gamma^i_{0j} = \Gamma^i_{j0} = \frac{1}{2}\partial_0 h_{ij},$$

$$\text{and} \quad \Gamma^i_{jk} = \frac{1}{2}(\partial_k h_{ij} + \partial_j h_{ik} - \partial_i h_{jk}). \qquad (5)$$

The worldlines of the Earth $[x^\mu_E(t) = (t, 0)]$ and star $[x^\mu_S(t) = (t, x^i_S)]$ are geodesics in both the unperturbed $(\eta_{\mu\nu})$ and perturbed $(\eta_{\mu\nu} + h_{\mu\nu})$ metrics; these worldlines are unaffected by the GW. However, the null geodesics $x^\mu_{t_0}(\lambda)$ and the tetrads $\epsilon^\mu_{\hat{a}}$ and $\sigma^\mu_{\hat{a}}$ are affected, and so are the tetrad components $p_{\hat{a}}$ defined in Eq. (2).

First, consider the tetrad along the Earth's worldline; this is perturbed $\epsilon^\mu_{\hat{a}} \mapsto \epsilon^\mu_{\hat{a}} + \delta\epsilon^\mu_{\hat{a}}(t)$ according to the parallel transport equations (the 4-velocity is $\epsilon^\mu_{\hat{0}}$),

$$\frac{\mathrm{d}}{\mathrm{d}t}\delta\epsilon^\mu_{\hat{a}}(t) = -\Gamma^\mu_{\nu\rho}\epsilon^\nu_{\hat{a}}\epsilon^\rho_{\hat{0}} + \mathcal{O}(h^2), \qquad (6)$$

where the symbols $\Gamma^\mu_{\nu\rho}$ are to be understood as being evaluated along the worldline of the Earth, $x^\mu_E(t)$. When integrating Eq. (6) the constants of integration may be discarded as it is the time-dependent change in astrometric position which we ultimately seek to measure. Substituting for the connection coefficients from Eq. (5) and integrating Eq. (6) along the worldline of the observer shows that the only nonzero components of $\delta\epsilon^\mu_{\hat{a}}(t)$ are

$$\delta\epsilon^j_{\hat{i}}(t) = -\frac{1}{2}H^j{}_{\hat{i}}\exp(-i\omega t_0). \qquad (7)$$

Note that the time-like component of the tetrad is unaffected. Similar equations hold for the deviation $\delta\sigma^j_{\hat{i}}(t)$.

Second, consider the null geodesics and their tangents; these are perturbed $x^\mu \mapsto x^\mu + \delta x^\mu(\lambda)$ and $p^\mu \mapsto p^\mu + \delta p^\mu(\lambda)$ according to the geodesic equation,

$$\frac{\mathrm{d}^2}{\mathrm{d}\lambda^2}\delta x^\mu_{t_0}(\lambda) = \frac{\mathrm{d}}{\mathrm{d}\lambda}\delta p^\mu_{t_0}(\lambda) = -\Gamma^\mu_{\nu\rho}p^\nu p^\rho + \mathcal{O}(h^2). \qquad (8)$$

In the above equation the symbols $\Gamma^\mu_{\nu\rho}$ are to be understood as being evaluated along the unperturbed trajectory $x^\mu_{t_0}(\lambda)$ (corrections to this trajectory enter at order of h^2). Substituting for the connection coefficients from Eq. (5) and for the metric perturbation from Eq. (3) gives

$$\frac{\mathrm{d}}{\mathrm{d}\lambda}\delta p^0_{t_0}(\lambda) = \frac{i\omega\Omega^2}{2}H_{ij}n^i n^j f(t_0, \lambda), \qquad (9a)$$

$$\frac{\mathrm{d}}{\mathrm{d}\lambda}\delta p^i_{t_0}(\lambda) = \frac{i\omega\Omega^2}{2}(-2H^i{}_j n^j + (q_j H^i{}_k + q_k H^i{}_j \\ - q^i H_{jk})n^j n^k)f(t_0, \lambda), \qquad (9b)$$

where $f(t_0, \lambda) = \exp(-i\omega\Omega\lambda(1 - q^i n_i) - i\omega t_0)$. Provided $q^i n_i \neq 1$, integrating Eq. (9a) with respect to λ with the

initial condition that the emission frequency in the rest frame of the star is unaffected by the GW $[\Omega_{\text{emit}} \equiv \eta_{\mu\nu}\sigma^\mu_{\hat{0}}p^\nu = \Omega$, which reduces to $\delta p^0_{t_0}(\lambda_S) = 0$ because $\delta\sigma^\mu_{\hat{0}} = 0]$ gives

$$\delta p^0(\lambda) = \frac{-\Omega}{2(1 - q^k n_k)}H_{ij}n^i n^j(f(t_0, \lambda) - f(t_0, \lambda_s)). \qquad (10)$$

Integrating Eq. (9b) twice with respect to λ gives

$$\delta x^i(\lambda) = \frac{-i}{2\omega(1 - q^l n_l)^2} \\ \times (-2H^i{}_j n^j + (q_j H^i{}_k + q_k H^i{}_j - q^i H_{jk})n^j n^k) \\ \times f(t_0, \lambda) + \lambda A^i + B^i, \qquad (11)$$

where A^i and B^i are constants of integration. The boundary conditions needed to determine A^i and B^i are as follows:

(a) The family of geodesics $x^\mu_{t_0}(\lambda) + \delta x^\mu_{t_0}(\lambda)$ remain null; at leading order this condition becomes

$$h_{\mu\nu}(\Omega\lambda + t_0, -\Omega\lambda n^i)p^\mu p^\nu + 2\eta_{\mu\nu}p^\mu \delta p^\nu_{t_0}(\lambda) = 0. \qquad (12)$$

(b) The geodesics intersect the Earth's worldline: the freedom to reparametrize the geodesics $\lambda \mapsto \lambda + \lambda_0$ may be used to ensure that the intersection occurs at $\lambda = 0$, so this condition becomes $\delta x^i_{t_0}(0) = 0$.

(c) The geodesics intersect the star's worldline at some value $\lambda_S + \delta\lambda_S$ [where $\delta\lambda_S = \mathcal{O}(h)$], so this condition becomes $x^i_{t_0}(\lambda_S + \delta\lambda_S) + \delta x^i_{t_0}(\lambda_S + \delta\lambda_S) = x^i_S$.

Boundary condition (b) fixes the constants B^i leaving

$$\delta x^i(\lambda) = \frac{-i}{2\omega(1 - q^\ell n_\ell)^2}(-2H^i{}_j n^j + (q_j H^i{}_k + q_k H^i{}_j \\ - q^i H_{jk})n^j n^k)(f(t_0, \lambda) - f(t_0, 0)) + \lambda A^i. \qquad (13)$$

Next, we decompose $A^i = A^i_\perp + A^i_\parallel$ in parallel and perpendicular directions to n^i. It is sufficient to enforce condition (a) at $\lambda = \lambda_S$ [where it is most straightforward to do so because $\delta p^0_{t_0}(\lambda_S) = 0$] as the norm of a tangent is automatically preserved along a geodesic; this gives

$$A^i_\perp = \frac{-\Omega n^i}{2(1 - q^\ell n_\ell)}H_{jk}n^j n^k f(t_0, \lambda_S + q_k H^i{}_j). \qquad (14)$$

Finally, condition (c) is applied to fix $A^i_\parallel$ and $\delta\lambda_S$, although only the former is needed here,

$$A^i_\parallel = \frac{i}{2\lambda_S\omega(1-q^\ell n_\ell)^2}(2H^i{}_j n^j - (q_j H^i{}_k + q_k H^i{}_j$$
$$-q^i H_{ij})n^j n^k - 2n^i H_{jk}n^j n^k$$
$$+ n^i q^m n_m H_{jk}n^j n^k)(f(t_0,0) - f(t_0,\lambda_S)). \quad (15)$$

As discussed following Eq. (2), the observed frequency is given by the temporal tetrad component of the photon $\Omega_{\text{obs}} \equiv -p_{\hat{0}}$,

$$\Omega_{\text{obs}} = (\eta_{\mu\nu} + h_{\mu\nu}(t_0,0))(p^\mu + \delta p^\mu_{t_0}(0))(\epsilon^\nu_{\hat{0}} + \delta\epsilon^\nu_{\hat{0}}(t_0))$$
$$= \Omega\left(1 - \frac{H_{ij}n^i n^j}{2(1-q^k n_k)}(f(t_0,0) - f(t_0,\lambda_S))\right). \quad (16)$$

Therefore, the redshift, defined as $1 + z \equiv \Omega/\Omega_{\text{obs}}$, where Ω is the emitted frequency, is obtained from Eq. (16) as

$$z = \frac{n^i n^j}{2(1-q^k n_k)}(h_{ij}(\text{E}) - h_{ij}(\text{S})). \quad (17)$$

The redshift depends antisymmetrically on the metric perturbations at the "emission" and "absorption" events at the star and the Earth, respectively [$h_{ij}(\text{E}) \equiv H_{ij}f(t_0,0)$ and $h_{ij}(\text{S}) \equiv H_{ij}f(t_0,\lambda_s)$]. This symmetry arises from the end points of the integral along the null geodesic linking the star to the Earth. The redshift varies periodically in time due to the GW. This redshifting, applied to a distant pulsar, causes individual pulses to arrive at the Earth periodically early and late; it is this timing residual which is searched for by PTAs.

As discussed following Eq. (2), the star's astrometric position is given by $n_{\hat{i}} \equiv p_{\hat{i}}/p_{\hat{0}}$ where $p_{\hat{0}}$ is the negative of Ω_{obs} in Eq. (16) and

$$p_{\hat{i}} = (\eta_{\mu\nu} + h_{\mu\nu}(t_0,0))(p^\mu + \delta p^\mu_{t_0}(0))(\epsilon^\nu_{\hat{i}} + \delta\epsilon^\nu_{\hat{i}}(t_0)). \quad (18)$$

Combining the previous results gives the observed astrometric deflection of the star due to a plane GW; this is the same result as that found in Ref. [22] [their Eq. (36)] with minor changes in notation;

$$\delta n_{\hat{i}} = \left[\left(\left\{1 + \frac{i(2-q^r n_r)}{\omega\lambda_S\Omega(1-q^\ell n_\ell)}(1 - \exp(-i\omega\Omega\lambda_S(1-q^s n_s)))\right\}n_{\hat{i}}\right.\right.$$
$$\left.- \left\{1 + \frac{i}{\omega\lambda_S\Omega(1-q^\ell n_\ell)}(1 - \exp(-i\omega\Omega\lambda_S(1-q^s n_s)))\right\}q_{\hat{i}}\right)\frac{H_{jk}n^j n^k}{2(1-q^\ell n_\ell)}$$
$$\left.- \left\{\frac{1}{2} + \frac{i}{\omega\lambda_S\Omega(1-q^\ell n_\ell)}(1 - \exp(-i\omega\Omega\lambda_S(1-q^s n_s)))\right\}H_{\hat{i}j}n^j\right]\exp(-i\omega t_0). \quad (19)$$

As was found for the redshift, the deflection depends on the metric perturbations at the star and at the Earth; although not symmetrically. This loss of symmetry is because the deflection depends both on an integral along the null geodesic trajectory as per Eq. (9b), and an integral along the Earth's worldline as per Eq. (6).

In the PTA analysis of stochastic GW backgrounds it is common to drop the "pulsar term" (which is called the "star term" here). This is possible because in the limit where the GW wavelength is much shorter than the distance to the star, $\omega\lambda_S\Omega \gg 1$, the overlap reduction function (ORF) tends to the result obtained by simply ignoring the "pulsar term" in Eq. (17) [35].

In the astrometric case the "star terms" can also sometimes be neglected, albeit for slightly different reasons. Consider Eq. (19) in the distant source limit $\omega\lambda_S\Omega \gg 1$ (i.e., where the star is many GW wavelengths distant from the observer). At leading order, only the first term in each set of curly brackets remains, and the result becomes

$$\delta n_{\hat{i}} = \frac{1}{2}\left(\frac{n_{\hat{i}} - q_{\hat{i}}}{1-q^\ell n_\ell}h_{\hat{j}\hat{k}}(\text{E})n^{\hat{j}}n^{\hat{k}} - h_{\hat{i}\hat{j}}(\text{E})n^{\hat{j}}\right). \quad (20)$$

Notice that in this limit all dependence on $h_{ij}(\text{S})$ has been lost. Also notice that the distant-source limit was taken for the astrometric response of a single star, and not for the statistical response of a network (quantified via the ORF) as in the PTA case. In Eq. (20) all contractions have been written using tetrad components; hereafter the hat notation denoting tetrad components will be dropped, and the astrometric deflections in Eq. (20) will simply be denoted δn_i.

The sensitivity of Gaia to GWs comes largely from the fact that it observes a large number of stars. These stars are generally well separated (by many gravitational wavelengths), and therefore the small star terms will be uncorrelated between stars. At small angular separation many stars are at similar distances (star clusters); this needs consideration in any practical application. In contrast, the larger Earth term is correlated between all stars; it is this that Gaia will aim to detect. The independent star terms may be treated as an effective noise source in the experiment. Including all the individual "star terms" would slightly increase the sensitivity of Gaia to the lowest GW frequencies; however this would involve fitting for the distance to every observed star individually.

A problem occurs with the distant source limit of the astrometric deflection when the GW source is collinear with a star (i.e., when $q^i n_i = 1$); the expression in Eq. (20) will, in general, diverge. In fact, this is usually not a problem, because in GR the GW polarizations are transverse (i.e., $h_{ij} q^j = 0$) which ensures that Eq. (20) has a smooth limit as $n^i \rightarrow q^i$. However, the divergence is a problem when working with alternative polarizations with a longitudinal component (i.e., when $h_{ij} q^j \neq 0$). For the remainder of this paper we work with the distant-source limit in Eq. (20) whenever possible, and fall back on the full (nondivergent) expression in Eq. (19) when the distant-source-limit approximation breaks down.

For a transverse GW the distant-source limit does not diverge and we may study the fractional error in the distant-source approximation. The error is defined as

$$\delta = \frac{|\delta n_i - \delta n_i^{\mathrm{ds}}|}{|\delta n_i|}, \qquad (21)$$

where δn_i is given by Eq. (19), and δn_i^{ds} by Eq. (20). This quantity is plotted in Fig. 2 as a function of the distance to the source for two frequencies at the edges of Gaia's GW bandwidth, $(10^{-8} - 3 \times 10^{-7})$ Hz [25]. Also shown in Fig. 2 is the cumulative distribution of the distances to stars in the Gaia catalog. Figure 2 shows that even for the longest GW wavelengths of interest to Gaia the error $\delta < 10^{-2}$ for 90% of stars in the Gaia catalog. This justifies the use of the distant-source limit Eq. (20) whenever it is not divergent.
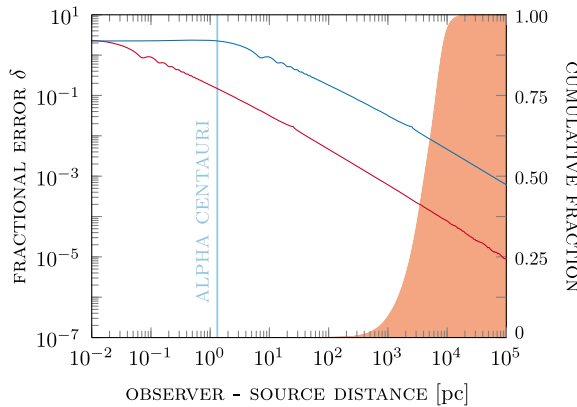

FIG. 2. The fractional error, δ [see Eq. (21)], in the distant-source approximation as a function of the distance to the star. The red and blue curves correspond to frequencies of 5×10^{-7} and 5×10^{-9} Hz respectively; these are the upper and lower frequency limits of Gaia's GW sensitivity [25]. Also shown on the secondary y axis is the cumulative distribution of distances to objects in the Gaia DR1 catalog (simulated distances to stars are taken from the Gaia Universe model snapshot [36]). The distant-source limit is a good approximation for the majority of stars in the catalog.

III. GRAVITATIONAL WAVE POLARIZATIONS

While GR only allows for two GW polarization modes (the transverse and traceless $+$ and $\times$ modes), alternative theories can include up to four additional modes. Besides the two GR modes, there may be a transverse trace scalar mode, two vectorial modes with mixed transverse and longitudinal components, and a purely longitudinal scalar mode. For a detailed discussion the reader is referred to Ref. [15].

In order to define the six GW polarization basis tensors we first introduce the orthonormal coordinate basis associated with the spherical polar coordinates (r, θ, ϕ);

$$\hat{e}_i^r = (\sin\theta\cos\phi, \sin\theta\sin\phi, \cos\theta), \qquad (22a)$$

$$\hat{e}_i^\theta = (\cos\theta\cos\phi, \cos\theta\sin\phi, -\sin\theta), \qquad (22b)$$

$$\hat{e}_i^\phi = (-\sin\phi, \cos\phi, 0). \qquad (22c)$$

The symmetric spatial GW polarization tensor, H_{ij}, for a GW traveling in direction $q_i = -\hat{e}_i^r$ can then be decomposed in terms of basis tensors as

$$H_{ij} = A_+ \epsilon_{ij}^+ + A_\times \epsilon_{ij}^\times + A_S \epsilon_{ij}^S + A_X \epsilon_{ij}^X + A_Y \epsilon_{ij}^Y + A_L \epsilon_{ij}^L, \qquad (23)$$

where the six GW basis tensors, ϵ_{ij}^P, are defined as

$$\epsilon_{ij}^+(q_k) = \hat{e}_i^\theta \hat{e}_j^\theta - \hat{e}_i^\phi \hat{e}_j^\phi, \qquad (24a)$$

$$\epsilon_{ij}^\times(q_k) = \hat{e}_i^\theta \hat{e}_j^\phi + \hat{e}_i^\phi \hat{e}_j^\theta, \qquad (24b)$$

$$\epsilon_{ij}^S(q_k) = \hat{e}_i^\theta \hat{e}_j^\theta + \hat{e}_i^\phi \hat{e}_j^\phi, \qquad (24c)$$

$$\epsilon_{ij}^X(q_k) = \hat{e}_i^\theta \hat{e}_j^r + \hat{e}_i^r \hat{e}_j^\theta, \qquad (24d)$$

$$\epsilon_{ij}^Y(q_k) = \hat{e}_i^\phi \hat{e}_j^r + \hat{e}_i^r \hat{e}_j^\phi, \qquad (24e)$$

$$\epsilon_{ij}^L(q_k) = \sqrt{2} \hat{e}_i^r \hat{e}_j^r. \qquad (24f)$$

The factor of $\sqrt{2}$ in the definition of $\epsilon_{ij}^L(q_k)$ is for normalization convenience and accounts for the fact that this tensor has only a single nonzero component, while all others have exactly two. In the standard Cartesian coordinate system the generalized perturbation tensor takes the form

$$H = \begin{pmatrix} A_+ + A_S & A_\times & A_X \\ A_\times & -A_+ + A_S & A_Y \\ A_X & A_Y & \sqrt{2} A_L \end{pmatrix}. \qquad (25)$$
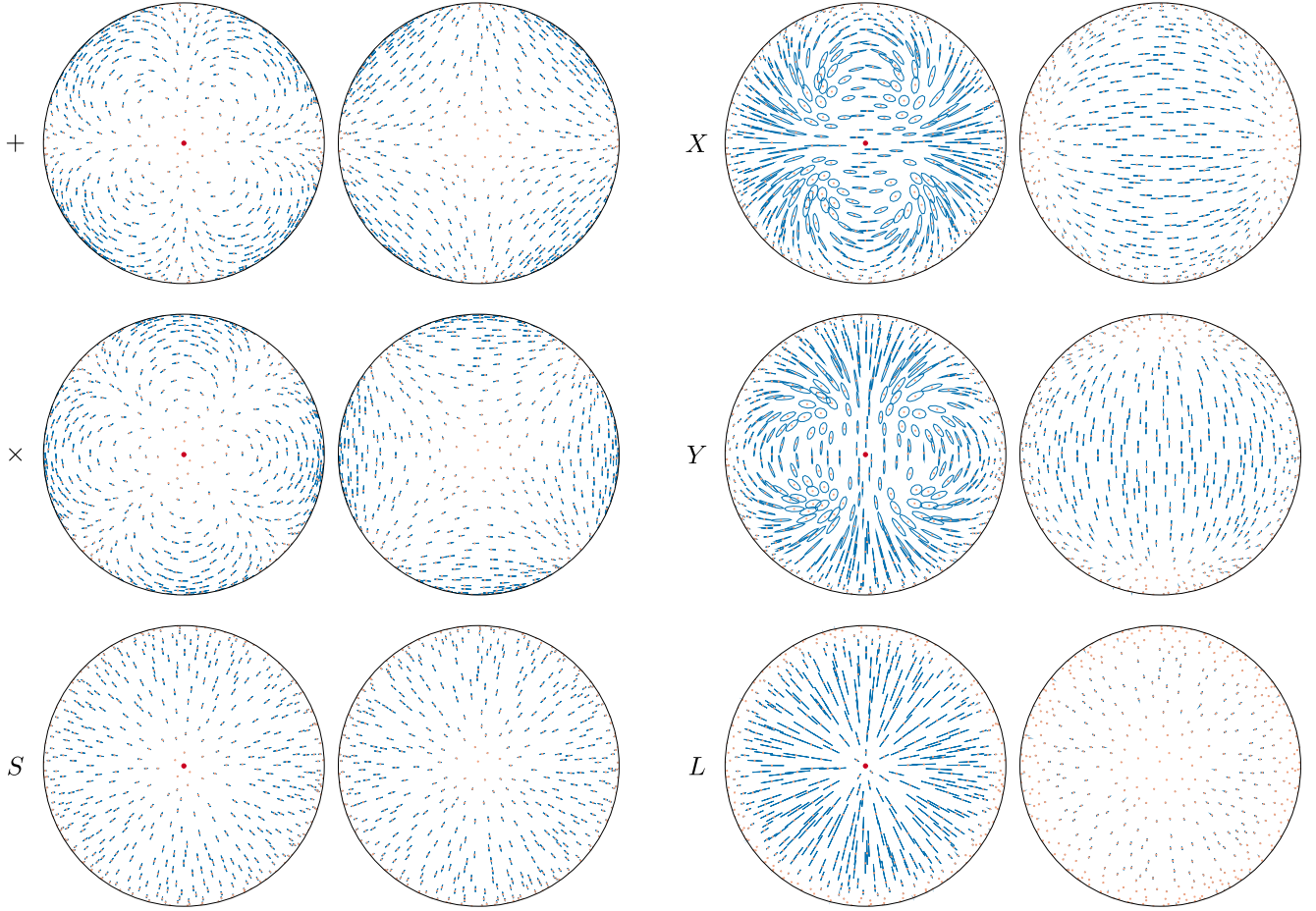
FIG. 3. Orthographic projections of the Northern (left) and Southern (right) hemispheres. Randomly placed on the sky are 1000 stars. A GW from a source located in the direction of the North pole (indicated by the red dots) is incident on the Earth causing the stars to move periodically at the GW frequency. The blue lines show the traces that each star would leave as it moves on the sky. For clarity, the incident GW has the unphysically large characteristic strain amplitude $A = 0.1$, and in the cases where the modes have longitudinal components (X, Y, and L), the star terms are included in the calculation of the astrometric deflection in order to avoid it becoming divergent near the North pole. In these latter three samples, all stars are placed at a distance of 10 gravitational wavelengths from the Earth. In reality, these neat elliptical patterns would appear more chaotic, since the distances to each star are generally different. The $+$ and $\times$ patterns are related to each other by a rotation through $\frac{\pi}{4}$ and the X and Y patterns are related by a rotation through $\frac{\pi}{2}$. The astrometric patterns for the two GR states including the star terms are presented additionally in Appendix A.

Shown in Fig. 3 are the distant-source limit astrometric deflection patterns for each of the three transverse GW polarization states, and the exact astrometric deflection patterns for the other three GW polarization modes with longitudinal components. The results in Fig. 3 were calculated using Eq. (20) for the $+$, $\times$, and S polarization states, and using Eq. (19) for the X, Y, and L states. Polarization tensors $H_{ij} = A_P \epsilon_{ij}^P$ with $A_P = 0.1$ (unrealistically large for visualization purposes) were used throughout, and in the latter three cases, all stars were placed 10 gravitational wavelengths away from Earth. If the distant-source limit were used for the three longitudinal modes, the plots would incorrectly show a divergence in the astrometric deflection pattern at the North pole due to the factor of $1 - q^\ell n_\ell$ in the denominator of Eq. (20).

IV. CORRELATED ASTROMETRIC DEFLECTIONS

In Sec. II of this article the astrometric response to a single monochromatic GW was derived. In this section the astrometric response to a stochastic background of GWs is considered. A stochastic background of GWs generates a stochastic pattern of astrometric deflections over the sky which is highly correlated at large angular scales. The pattern of this correlation depends on the polarization of the GWs which make up the background. The general framework for considering correlated vector fields on the sphere is introduced, and then in Secs. IV A–IV D below, the correlations for several different combinations of the polarization states discussed in Sec. III are explicitly evaluated.

The discussion in this article is restricted to stochastic GW backgrounds which are Gaussian, stationary, isotropic and unpolarized (at this point we do not specify which polarization states comprise the background, just that they are uncorrelated with each other so the background is statistically unpolarized). The astrometric deflection is then a Gaussian random vector field on the sphere, and the statistical properties of this field are described by a correlation matrix. Adopting a convenient decomposition for this correlation matrix allows for an intuitive visualization of key features of the correlation over the sphere of the sky. This decomposition will also permit a clear comparison with the analogous calculations in the pulsar timing literature.

Consider the correlation between the astrometric deflections at two different points on the sky. The astrometric response is given by the distant-source limit formula, Eq. (20) (specific examples of when this formula is not valid will be considered later in this section). In this limit, the astrometric deflection depends only on the "Earth term" metric perturbation; this time-dependent metric perturbation can be Fourier decomposed as

$$h_{ij}(t) = \Re\left\{\sum_P \int_0^\infty df \int_{S^2} d\Omega_\mathbf{q} A_P(\mathbf{q}, f) e^{-2\pi i f t} \epsilon_{ij}^P(\mathbf{q})\right\},$$

$$(26)$$

where $f = \omega/2\pi$ is the linear GW frequency, $A_P(\mathbf{q}, f)$ are the (complex) Fourier coefficients, $d\Omega_\mathbf{q}$ is the area element on the sphere, and $\mathbf{q} \equiv q_i$ is the direction from which the GW originates. The label P indicates the GW polarization which, at this stage, may be any of the six states $P \in \{+, \times, S, X, Y, L\}$ described in Sec. III.

The GW background is assumed to be Gaussian, zero-mean, stationary, isotropic, and unpolarized. The expectation values of the Fourier coefficients in such a background satisfy

$$\langle A_P(\mathbf{q}, f) A_{P'}^*(\mathbf{q}', f') \rangle = C(f) \delta_{PP'} \delta_{S^2}(\mathbf{q}, \mathbf{q}') \delta(f - f'),$$

$$(27a)$$

$$\langle A_P(\mathbf{q}, f) A_{P'}(\mathbf{q}', f') \rangle = 0,$$

$$(27b)$$

where the function $C(f)$ is related to the spectral energy density in the GW background [37].

The astrometric deflection is linear in the metric perturbation, and the response to each Fourier mode may be calculated individually:

$$\delta n_i(\mathbf{n}, t) = \Re\left\{\sum_P \int_0^\infty df e^{-2\pi i f t} \int_{S^2} d\Omega_\mathbf{q} A_P(\mathbf{q}, f)\right.$$

$$\left. \times \Delta_{i}{}^{jk}(\mathbf{n}, \mathbf{q}) \epsilon_{jk}^P(\mathbf{q})\right\},$$

$$(28)$$

where we have defined

$$\Delta_{i}{}^{jk}(\mathbf{n}, \mathbf{q}) = \frac{1}{2}\left(\frac{n_i - q_i}{1 - q^\ell n_\ell} n^j n^k - \delta_{i}{}^j n^k\right).$$

$$(29)$$

The linearity of the astrometric deflection with the metric perturbation also ensures that it will be a Gaussian random variable, and that its statistical properties depend only on the two-point correlation. Using Eqs. (27) and (28), it is straightforward to show that the expectation of the product of astrometric responses δn_i and δm_i of two stars, situated at two different points on the sky, n_i and m_i, separates into a factor depending on the measurement times and a factor depending on the locations of the stars on the sky,

$$\langle \delta n_i(\mathbf{n}, t) \delta m_j(\mathbf{m}, t') \rangle = T(t, t') \Gamma_{ij}(\mathbf{n}, \mathbf{m}).$$

$$(30)$$

Because both $\delta n_i(\mathbf{n}, t)$ and $\delta m_j(\mathbf{m}, t)$ have zero mean, this expectation is proportional to the correlation between the two quantities. As is well known, the temporal correlation factor is given by the cosine transform of the GW frequency spectrum:

$$T(t, t') = \frac{1}{4}\int_0^\infty df C(f)(e^{2\pi i f(t-t')} + e^{-2\pi i f(t-t')}). \quad (31)$$

The spatial correlation factor is a sum of integrals of products of vectors over the sphere for each mode P [cf. the factor of $\delta_{PP'}$ in Eq. (27a)]:

$$\Gamma_{ij}(\mathbf{n}, \mathbf{m}) = \sum_P \Gamma_{ij}^P(\mathbf{n}, \mathbf{m}),$$

$$(32)$$

where, for each polarization state, we defined

$$\Gamma_{ij}^P(\mathbf{n}, \mathbf{m}) = \int_{S^2} d\Omega_\mathbf{q} \delta n_i^P(\mathbf{n}, \mathbf{q}) \delta m_j^P(\mathbf{m}, \mathbf{q}), \quad (33)$$

$$\text{where } \delta n_i^P(\mathbf{n}, \mathbf{q}) = \Delta_{i}{}^{jk}(\mathbf{n}, \mathbf{q}) \epsilon_{jk}^P(\mathbf{q}). \quad (34)$$

Only the spatial part of the correlation, $\Gamma_{ij}(\mathbf{n}, \mathbf{m})$, depends on the polarization content of the GW background. Hereafter, only spatial correlations will be investigated.

Since the background is isotropic, the sky sphere can be rotated into the most convenient orientation. The first star, n_i, is placed at the North Pole, and the second, m_i, in the x-z plane (for anisotropic backgrounds, this transformation is still possible, though in that case the background needs to also be rotated into the new frame; see Ref. [33] for details). The stars have coordinates

$$\mathbf{n} = (0, 0, 1),$$

$$(35a)$$

$$\mathbf{m} = (\sin \Theta, 0, \cos \Theta).$$

$$(35b)$$

The astrometric deflection vectors lie in the tangent plane of the sphere; it is now necessary to introduce a pair of basis vectors at both points on the sphere. The choice of basis is of course arbitrary; however, the following choice will prove to be convenient. For any pair of points n_i and m_i there is a unique (shortest) geodesic, γ, linking n_i to m_i; at both n_i and m_i the unit tangent vector to γ and the unit vector pointing to the left of γ form an orthonormal basis. For the values of n_i and m_i in Eqs. (35a)–(35b) the coordinate expressions for these basis vectors are

$$\hat{u}^x = (1, 0, 0), \tag{36a}$$

$$\hat{u}^y = (0, 1, 0), \tag{36b}$$

$$\hat{u}^\theta = (\cos\Theta, 0, -\sin\Theta), \tag{37a}$$

$$\hat{u}^\phi = (0, 1, 0), \tag{37b}$$

while the general definitions for two arbitrary points on the sphere are

$$\hat{u}^x = \frac{(\hat{n} \times \hat{m}) \times \hat{n}}{\sqrt{1 - (\hat{n} \cdot \hat{m})^2}}, \tag{38a}$$

$$\hat{u}^y = \frac{\hat{n} \times \hat{m}}{\sqrt{1 - (\hat{n} \cdot \hat{m})^2}}, \tag{38b}$$

$$\hat{u}^\theta = \frac{(\hat{n} \times \hat{m}) \times \hat{m}}{\sqrt{1 - (\hat{n} \cdot \hat{m})^2}}, \tag{39a}$$

$$\hat{u}^\phi = \frac{\hat{n} \times \hat{m}}{\sqrt{1 - (\hat{n} \cdot \hat{m})^2}}. \tag{39b}$$

The geometric setup is illustrated in Fig. 4.

The astrometric deflections may now be decomposed into this basis:

$$\delta n_i^P(\mathbf{q}) = \delta n_x^P(\mathbf{q})\hat{u}_i^x + \delta n_y^P(\mathbf{q})\hat{u}_i^y, \tag{40a}$$

$$\delta m_i^P(\mathbf{q}) = \delta m_\theta^P(\mathbf{q})\hat{u}_i^\theta + \delta m_\phi^P(\mathbf{q})\hat{u}_i^\phi, \tag{40b}$$

where the scalar coefficients are given by

$$\delta n_x^P(\mathbf{q}) = \delta n_i^P(\mathbf{q})\hat{u}_x^i, \tag{41a}$$

$$\delta n_y^P(\mathbf{q}) = \delta n_i^P(\mathbf{q})\hat{u}_y^i, \tag{41b}$$

$$\delta m_\theta^P(\mathbf{q}) = \delta m_i^P(\mathbf{q})\hat{u}_\theta^i, \tag{42a}$$

$$\delta m_\phi^P(\mathbf{q}) = \delta m_i^P(\mathbf{q})\hat{u}_\phi^i. \tag{42b}$$

Substituting Eqs. (40a)–(40b) into Eq. (33) and expanding gives an expression for the spatial correlation function as a sum of scalar integrals over the sphere,
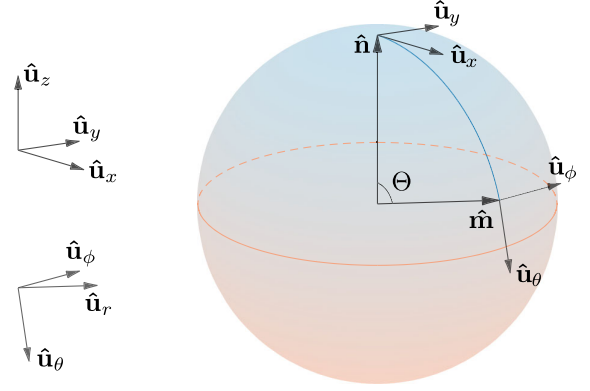

FIG. 4. Geometrical setup of the vectors involved in the calculation of the overlap reduction functions. A pair of stars, one of them nominally placed at the North pole, and a second one at angular separation Θ (along the arc $\phi = 0$) are considered. Each of them experiences astrometric response due to a background of gravitational radiation. On the left-hand side of the figure are shown the Cartesian triad associated with the point $\hat{n}^i$ (top) and the curvilinear triad associated with the point $\hat{m}^i$ (bottom). The astrometric deflection at point $\hat{n}^i$ ($\hat{m}^i$) is a vector in the tangent plane to the sphere, and can be decomposed in terms of just $\hat{e}_x$ and $\hat{e}_y$ ($\hat{e}_\theta$ and $\hat{e}_\phi$). We are interested in the correlations between these vector components.

$$\Gamma_{ij}^P(\Theta) = \hat{u}_i^x\hat{u}_j^\theta \int_{S^2} d\Omega_{\mathbf{q}} \delta n_x^P(\mathbf{q})\delta m_\theta^P(\mathbf{q}) \tag{43a}$$

$$+ \hat{u}_i^x\hat{u}_j^\phi \int_{S^2} d\Omega_{\mathbf{q}} \delta n_x^P(\mathbf{q})\delta m_\phi^P(\mathbf{q}) \tag{43b}$$

$$+ \hat{u}_i^y\hat{u}_j^\theta \int_{S^2} d\Omega_{\mathbf{q}} \delta n_y^P(\mathbf{q})\delta m_\theta^P(\mathbf{q}) \tag{43c}$$

$$+ \hat{u}_i^y\hat{u}_j^\phi \int_{S^2} d\Omega_{\mathbf{q}} \delta n_y^P(\mathbf{q})\delta m_\phi^P(\mathbf{q}). \tag{43d}$$

In fact, it can be shown that for any correlated vector field on the sphere which is statistically invariant under both rotations and parity transformations the $y - \theta$ and $x - \phi$ terms [i.e., Eqs. (43b) and (43c)] vanish. These terms can also explicitly be shown to vanish for each GW polarization considered individually in Secs. IV A–IV D below. Therefore, remarkably, the full spatial correlation matrix is always fully specified by just two real-valued functions, and may be written as

$$\Gamma_{ij}^P(\mathbf{n}, \mathbf{m}) = \Gamma_{x\theta}^P(\Theta)\hat{u}_i^x\hat{u}_j^\theta + \Gamma_{y\phi}^P(\Theta)\hat{u}_i^y\hat{u}_j^\phi, \tag{44}$$

where $\Theta = \arccos(\mathbf{n} \cdot \mathbf{m})$, the unit vectors are defined in terms of n_i and m_i in Eqs. (38a)–(38b) and (39a)–(39b) and the functions $\Gamma_{x\theta}^P(\Theta)$ and $\Gamma_{y\phi}^P(\Theta)$ are defined as the integrals in Eqs. (43a) and (43d) respectively. This result is the equivalent of Eq. (71) in Ref. [22].

One advantage of the decomposition of the spatial correlation matrix in Eq. (44) is that the functions $\Gamma_{x\theta}^P(\Theta)$

and $\Gamma^P_{y\phi}(\Theta)$ have the clear interpretation as the *scalar* correlations of the "parallel" and "perpendicular" components of the astrometric deflection. Here "parallel" means tangent to the geodesic linking the two points, and "perpendicular" means pointing to the left of this curve; see Fig. 4.

It is well known that any vector field v_i on the sphere admits a unique Helmholtz decomposition into gradient and curl parts; $v_i = \nabla_i \phi + (\nabla \wedge)_i \psi$, where ∇ is the surface gradient on the sphere, $(\nabla \wedge) = \mathbf{r} \wedge \nabla$ is the surface curl, and ϕ and ψ are scalar fields on the sphere. Another advantage of the spatial correlation matrix in Eq. (44) is that the functions $\Gamma^P_{x\theta}(\Theta)$ and $\Gamma^P_{y\phi}(\Theta)$ govern the statistical properties of the gradient and curl parts respectively. By comparing components, it can be seen that the $\Gamma^P_{x\theta}(\Theta)$ and $\Gamma^P_{y\phi}(\Theta)$ terms in Eq. (44) are exactly the general divergence and curl kernels Ψ_{div} and Ψ_{curl} defined in Ref. [38]. A random vector field described by a spatial correlation matrix with $\Gamma_{y\phi} = 0$ will be a pure divergence, and a vector field described by a correlation matrix with $\Gamma_{x\theta} = 0$ will be a pure curl.

A. Tensorial transverse-traceless polarizations

This section considers the astrometric correlations arising in a background of just the two GR polarization modes; i.e., $P \in \{+, \times\}$. This calculation was considered previously in Ref. [22]; here this result is reproduced within the framework outlined in the previous section.

In Appendix B it is shown how to evaluate the integrals $\Gamma^+_{x\theta}$, $\Gamma^+_{y\phi}$, $\Gamma^\times_{x\theta}$, and $\Gamma^\times_{y\phi}$ defined in Eq. (33). Following Eq. (32), the spatial correlation matrix in a background with multiple polarizations is the sum of the individual spatial correlations, so $\Gamma^{+,\times}_{x\theta}(\Theta) = \Gamma^+_{x\theta}(\Theta) + \Gamma^\times_{x\theta}(\Theta)$, and similarly for $\Gamma^{+,\times}_{y\phi}(\Theta)$. Remarkably, these two functions turn out to be equal in this particular case,

$$\mathcal{T}(\Theta) = \Gamma^{+,\times}_{x\theta}(\Theta) = \Gamma^{+,\times}_{y\phi}(\Theta) = \frac{2\pi}{3} - \frac{14\pi}{3}\sin^2(\Theta/2)$$
$$- 8\pi \frac{\sin^4(\Theta/2)}{1 - \sin^2(\Theta/2)}\ln(\sin(\Theta/2)). \quad (45)$$

Throughout this section all correlation functions are written in terms of $\sin(\Theta/2)$. Therefore, the correlated astrometric deflection field generated by a Gaussian, stationary, isotropic, unpolarized GW background in GR is fully specified by a single real-valued function of the angular separation on the sphere, $\mathcal{T}(\Theta)$.

This function ought to be compared to the corresponding result for pulsar timing. The spatial correlation between the redshift at two different points on the sky is given by the well-known Hellings-Downs curve [39],

$$\mathcal{H}(\Theta) = \frac{1}{2}(1 + \beta) - \frac{1}{4}\sin^2(\Theta/2)$$
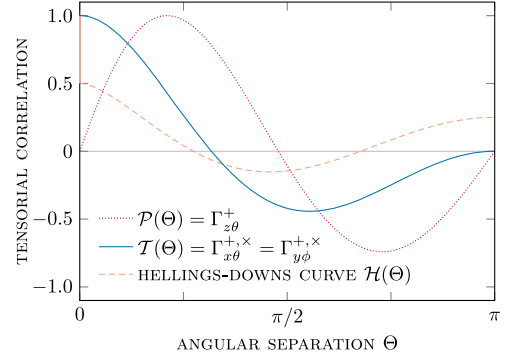$$+ 3\sin^2(\Theta/2)\ln(\sin(\Theta/2)), \quad (46)$$

FIG. 5. The astrometric and redshift correlations as a function of angular separation on the sky in a background of tensorial, transverse-traceless GWs (i.e., + and ×). The well-known Hellings-Downs curve, $\mathcal{H}(\Theta)$, determines the redshift correlations and is shown here with the usual normalization $\lim_{\Theta \to 0} H(\Theta) = \frac{1}{2}$ due to the presence of the pulsar term in Eq. (17). The astrometric correlations are similarly determined by a single function, $\mathcal{T}(\Theta)$, which is shown with the normalization $\mathcal{T}(0) = 1$ as there is no star term in Eq. (20). The function $\mathcal{T}(\Theta)$ is the astrometric analog of the Hellings-Downs curve. The function $\mathcal{P}(\Theta)$ is the redshift-astrometry analog of the Hellings-Downs curve and is introduced and discussed in Sec. V.

where $\beta = 1$ for colocated pulsars and is zero otherwise. The standard PTA normalization is $\lim_{\Theta \to 0} \mathcal{H}(\Theta) = \frac{1}{2}$; the β in Eq. (46) comes from the expectation of the pulsar terms in Eq. (17) which is nonzero only for the autocorrelation. In the astrometric case there are no star terms [see Eq. (20)], so in the case of a total time correlation $[T(t, t') = 1]$, the normalization $\mathcal{T}(0) = 1$ can be chosen. Regardless, it is the "shape" of these curves that is of most interest here.

The well-known Hellings-Downs curve governs the spatial correlation of the redshift on the sky. Similarly, the function $\mathcal{T}(\Theta)$ governs the spatial correlation of the astrometric deflection on the sky. The function $\mathcal{T}(\Theta)$ can therefore be considered as the astrometric analog of the Hellings-Downs curve. Both $\mathcal{T}(\Theta)$ and $\mathcal{H}(\Theta)$ are shown in Fig. 5.

In order to gain a better understanding of what this vector field correlation over the sky means it is useful to draw a realization of this random process and to plot the result. The results are shown in Fig. 6, and an overview of the procedure used to produce the data in this plot can be found in Appendix C.

B. Scalar "breathing" polarization

The astrometric correlations arising in a background of transverse scalar GWs (i.e., $P \in \{S\}$) are considered here. Appendix D shows how to evaluate the integrals $\Gamma^S_{x\theta}$ and $\Gamma^S_{y\phi}$ defined in Eq. (33); here only the results of these integrals are presented:
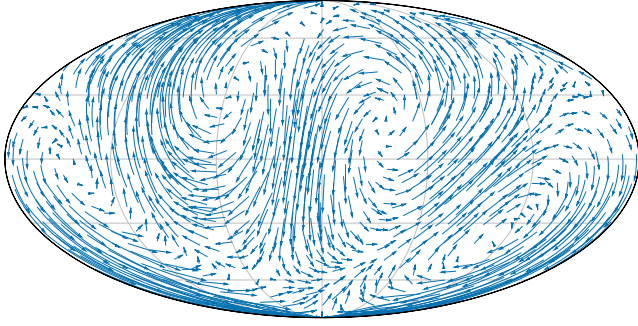
FIG. 6. A random realization of the astrometric deflection field for a background of tensorial + and × waves. The position of each star is recorded twice, separated by a time Δt. These two positions are shown here (in a Mollweide projection) at the foot and head respectively of each arrow. The length of each arrow is proportional to the total power in the GW background at frequencies $f < 1/\Delta t$. The length of the arrows has been greatly scaled up here for clarity.

$$\Gamma^S_{x\theta}(\Theta) = \frac{\pi}{3}\cos\Theta \equiv \frac{\pi}{3} - \frac{2\pi}{3}\sin^2(\Theta/2), \quad (47a)$$

$$\Gamma^S_{y\phi}(\Theta) = \frac{\pi}{3}. \quad (47b)$$

Again, this should be compared to the PTA result for the redshift correlation in a stochastic background of "breathing" GWs. This was derived in Ref. [16] as

$$\mathrm{corr}(\Theta) = \frac{1}{2}(1+\beta) + \frac{1}{2} - \frac{1}{4}\sin^2(\Theta/2), \quad (48)$$

where the variable β is defined just after Eq. (46). All three of these functions are plotted in Fig. 7.

The most surprising aspect of astrometric correlation is the result for $\Gamma^S_{y\phi}(\Theta)$; the "perpendicular" components of
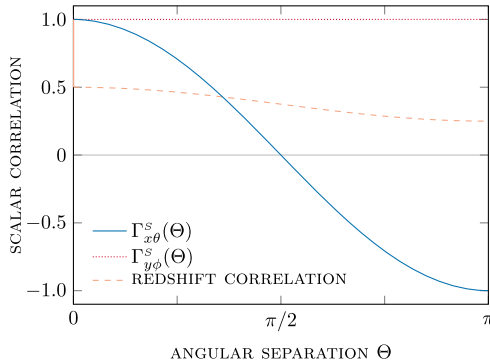

FIG. 7. The astrometric and redshift correlations as a function of angular separation on the sky in a background of scalar, "breathing" GWs (i.e., S). The functions which determine the astrometric correlations [$\Gamma^S_{x\theta}(\Theta)$ and $\Gamma^S_{y\phi}(\Theta)$; see Eq. (47)] are normalized so that their maximum is unity. The PTA result for the correlated redshift in Eq. (48) is plotted, normalized to $\frac{1}{2}$ at $\Theta = 0$.
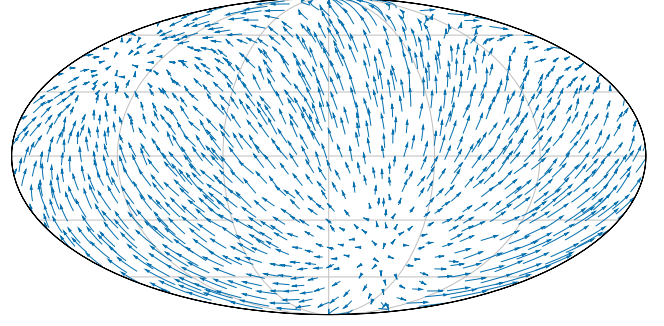
FIG. 8. A random realization of the astrometric deflection field for a background of scalar "breathing" S waves. This was produced in the same way as Fig. 6. It is clear from the plot that the astrometric deflection vector field has a random dipole-like structure on the sphere; the origin of this behavior is the fact that $\Gamma^S_{y\phi}(\Theta) \equiv$ const, and the astrometric deflection at any two points on the sky are perfectly correlated.

the astrometric deflection at any two points on the sky are always *perfectly* correlated. This is an extremely strong constraint which any allowed realizations of the vector field must obey. The interpretation of this becomes clearer when a random realization of the correlation is drawn; this is shown in Fig. 8.

The random realizations of the astrometric deflections plotted in Figs. 6 and 8 are qualitatively different. The transverse-traceless polarizations of GR produce a distinctive curl-like pattern at large angular scales, whereas the transverse-trace (or scalar) mode generates a dipole-like structure on the sky. The polarization content of the stochastic GW background determines the spatial correlations among the astrometric deflections. If Gaia, or some other future astrometry mission, is able to measure the stochastic pattern of astrometric deflections due to a background of GWs, the measured correlations will encode details of the polarization content of the background and thereby enable a test of GR.

C. Vectorial polarizations

After analyzing the tensorial modes and the scalar "breathing" mode, it is interesting to consider the astrometric correlations arising in a background of just the two vectorial polarization modes; i.e., $P \in \{X, Y\}$. These calculations have an additional complication over those in the preceding sections as the vectorial polarizations have a longitudinal component which introduces a singularity into the "Earth term"-only redshift and astrometric responses [see Eqs. (17) and (20)]. In the case of the redshift correlation, as was found in Ref. [16], this means the correlation curve diverges at $\Theta = 0$;

$$\Gamma^{X,Y}_z(\Theta) = -\frac{28\pi}{3} + \frac{32\pi}{3}\sin^2(\Theta/2) - 8\pi\ln(\sin(\Theta/2)). \quad (49)$$
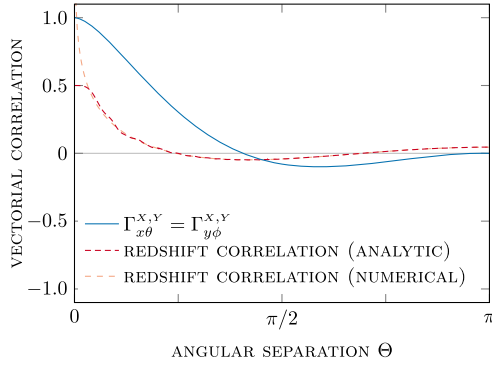
FIG. 9. The astrometric and redshift correlations as a function of angular separation on the sky in a background of vectorial GWs (i.e., $P \in \{X, Y\}$). The function which determines the astrometric correlation $[\Gamma_{x\theta}^{X,Y}(\Theta) = \Gamma_{y\phi}^{X,Y}(\Theta)$; see Eq. (50)] is normalized so that its maximum is unity. The numerical redshift result [for pulsars at distances $(100\lambda_{\mathrm{GW}}, 200\lambda_{\mathrm{GW}})$] for the correlated redshift is plotted (normalized to $\frac{1}{2}$ at $\Theta = 0$) along with the divergent result from Eq. (49).
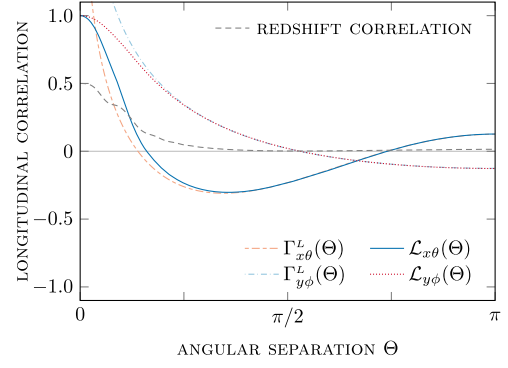

FIG. 10. The astrometric and redshift correlations as a function of angular separation on the sky in a background of scalar longitudinal GWs (i.e., L). The numerical curves which determine the astrometric correlation $[\mathcal{L}_{x\theta}(\Theta)$ and $\mathcal{L}_{y\phi}(\Theta)$; see Appendix F 1] are normalized so that their maximum is unity; the two analytical divergent curves $\Gamma_{x\theta}^{L}(\Theta)$ and $\Gamma_{y\phi}^{L}(\Theta)$ [see Eq. (51)] are also plotted. The numerical redshift result for the correlated redshift is plotted, normalized to $\frac{1}{2}$ at $\Theta = 0$.

This result is plotted in Fig. 9. The divergence at the origin is a result of the use of the "Earth term"-only redshift response. If the "star term" is included the result becomes finite, and the correlation depends on the distance to the star. When including the star term the integration must be performed numerically; the results of this numerical integration are also shown in Fig. 9 for two pulsars at distances of 100 and 200 gravitational wavelengths respectively.

In contrast, the divergence in the astrometric response is of a logarithmic nature [i.e., of the type $\int \mathrm{d}x f(x)/x$], and is regularized by the integral over the sky. This means that the resulting correlation curve is nondivergent, even though the two individual astrometric responses do diverge. Appendix E discusses how to evaluate the integrals $\Gamma_{x\theta}^{X}$, $\Gamma_{y\phi}^{X}$, $\Gamma_{x\theta}^{Y}$, and $\Gamma_{y\phi}^{Y}$ analytically. Following Eq. (32), the spatial correlation matrix in a background with multiple polarizations is the sum of the individual spatial correlations, $\Gamma_{x\theta}^{X,Y}(\Theta) = \Gamma_{x\theta}^{X}(\Theta) + \Gamma_{x\theta}^{Y}(\Theta)$, and similarly for $\Gamma_{y\phi}^{X,Y}(\Theta)$. Again, these two functions turn out to be equal:

$$\Gamma_{x\theta}^{X,Y}(\Theta) = \Gamma_{y\phi}^{X,Y}(\Theta) = \frac{4\pi}{3} + \frac{8\pi}{3}\sin^2(\Theta/2)$$
$$+ 8\pi \frac{\sin^2(\Theta/2)}{1 - \sin^2(\Theta/2)} \ln(\sin(\Theta/2)). \quad (50)$$

This vectorial astrometric correlation function is also plotted in Fig. 9.

D. Scalar "longitudinal" polarization

The scalar longitudinal mode, on the other hand, is more interesting, as in this case the "Earth term"-only astrometric correlation curves do diverge at $\Theta = 0$. These functions are

given by (see Appendix F for details of the evaluation of the relevant integrals, and Fig. 10 for plots of the two functions)

$$\Gamma_{x\theta}^{L}(\Theta) = -\frac{10\pi}{3} + \frac{8\pi}{3}\sin^2(\Theta/2) - 2\pi \frac{\ln(\sin(\Theta/2))}{1 - \sin^2(\Theta/2)},$$
$$(51a)$$

$$\Gamma_{y\phi}^{L}(\Theta) = -\frac{4\pi}{3} - 2\pi \frac{\ln(\sin(\Theta/2))}{1 - \sin^2(\Theta/2)}. \quad (51b)$$

Similarly to the vectorial redshift correlation, the divergence is a result of using the "Earth term"-only astrometric response in Eq. (20). If instead, the full astrometric response in Eq. (19) is used the correlation is finite, although the integrals need to be evaluated numerically in this case (see Appendix F 1 for details). When using the full astrometric response, the correlation curves depend on the distance to the stars; two such curves are shown in Fig. 10 for stars at distances of 100 and 200 gravitational wavelengths.

One conclusion which can be drawn from the curves in Fig. 10 is that for a longitudinally polarized GW background there are only strong astrometric correlations between stars at small angular separations. This is in marked contrast to the GR case of a tensorial $\{+, \times\}$ background, where correlations of order unity persist at all angular scales.

In order to better understand the behavior at $\Theta = 0$, it is useful to consider the full (nondivergent) correlation including the distances to the stars at the point $\Theta = 0$. At this point the full integral can be evaluated analytically, giving a correlation which is a function of just the distances d_n and d_m to the two stars. This function quantifies the
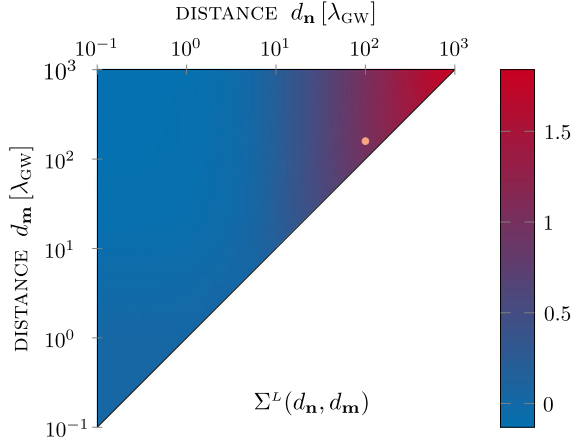
FIG. 11. Surface plot of the astrometric longitudinal correlation at $\Theta = 0$, given by $\Sigma^L(d_\mathbf{n}, d_\mathbf{m})$ for $d_\mathbf{m} \geq d_\mathbf{n}$ [see Eq. (F7) in Appendix F 2 for the precise expression]. The two distances are expressed in terms of gravitational wavelengths. A dot marks the point $(d_\mathbf{n}, d_\mathbf{m}) = (100, 200)$, which is used for computing the numerical integral in Fig. 10.

cross correlation of the deflections of two stars which appear at the same point on the sky, but are separated in distance by many gravitational wavelengths. A plot of this function is given in Fig. 11 and an explicit expression for it is given in Appendix F 2.

V. REDSHIFT-ASTROMETRY CORRELATIONS

As discussed above, a stochastic background of GWs can, in principle, be detected by both pulsar timing or astrometric measurements. However, improved sensitivities can be obtained by combining these two techniques. In addition to the straightforward increase in signal to noise that comes with the increased amount of data, there is an additional benefit that comes from now being able to search for GWs in the cross correlation between the two data sets. It is this redshift-astrometric correlation which is considered here.

As described above, an isotropic, unpolarized background of GWs causes a correlated redshift pattern on the sky. The correlation at two points on the sky is described by a single real-valued function of the angular separation [$\mathcal{H}(\Theta)$; see Eq. (46) and Fig. 5] known as the Hellings-Downs curve [39]. This result is a very robust prediction within GR; it depends only on the existence of the two polarizations predicted by the theory and the homogeneity and isotropy of the Universe on scales comparable to the distance to the GW sources. It does not depend on the dynamics of the individual sources generating the background. The detection of a Hellings-Downs correlated redshift pattern via pulsar timing would be clear evidence for a stochastic GW background.

Similarly, a background of GWs causes a correlated astrometric deflection pattern on the sky. This correlation

pattern is also fully specified by a single real-valued function of the angular separation [$\mathcal{T}(\Theta)$; see Eq. (45) and Fig. 5] which was first derived in Ref. [22], although not in the current form. This is the astrometric analog of the Hellings-Downs curve; it is a similarly robust prediction of GR and the detection of this pattern via astrometric measurements would provide similarly clear evidence for a stochastic GW background.

Additionally, there is a correlation between the redshift and astrometric deflection. The redshift of a pulsar in direction $\mathbf{n}$ is correlated with the astrometric deflection, $\delta m_i = \delta m_\theta \hat{u}_i^\theta + \delta m_\phi \hat{u}_i^\phi$, of a star in direction $\mathbf{m}$ via

$$\langle z(\mathbf{n}) \delta m_i(\mathbf{m}) \rangle \propto \int d\Omega_\mathbf{q} z(\mathbf{n}) \delta m_i(\mathbf{m})$$

$$\propto \int d\Omega_\mathbf{q} z(\mathbf{n}) (\delta m_\theta \hat{u}_i^\theta + \delta m_\phi \hat{u}_i^\phi)$$

$$\propto \Gamma_{z\theta}(\Theta) \hat{u}_i^\theta + \Gamma_{z\phi}(\Theta) \hat{u}_i^\theta, \qquad (52)$$

where $\Theta = \arccos(\mathbf{n} \cdot \mathbf{m})$. General considerations again show that $\Gamma_{z\phi}$ always vanishes. For a GW background of $+$ and $\times$ waves the remaining function evaluates to

$$\mathcal{P}(\Theta) = \Gamma_{z\theta}^+(\Theta) = \frac{8\pi}{3} \sin(\Theta/2) \cos(\Theta/2)$$

$$+ 8\pi \frac{\sin^3(\Theta/2)}{\cos(\Theta/2)} \ln(\sin(\Theta/2)). \qquad (53)$$

The basis vectors $\hat{u}_i^\theta$ and $\hat{u}_i^\phi$ are defined in Sec. IV and illustrated in Fig. 4. From Eq. (52) it follows that the redshift of a pulsar is correlated with the "parallel component" of the astrometric deflection of a star, and is uncorrelated with the "perpendicular component" (see Fig. 4 for an illustration of the geometric setup).

Furthermore, the correlation between a pulsar and the response from a $\times$-polarized GW vanishes,

$$\Gamma_{z\theta}^\times(\Theta) = \Gamma_{z\phi}^\times(\Theta) = 0; \qquad (54)$$

therefore the entire correlation between the redshift of a pulsar and the astrometric deflection of a star for $P \in \{+, \times\}$ is governed by $\mathcal{P}(\Theta)$ in Eq. (53). This is shown, together with the other curves relevant to GR, in Fig. 5, and with the other redshift-astrometry curves in Fig. 12.

PTA-astrometry correlations like the one in Eq. (53) can be found for the other polarization states, too. In particular, the curves can be derived explicitly in the case of scalar "breathing" and vectorial modes,

$$\Gamma_{z\theta}^S(\Theta) = -\frac{20\pi}{3} \sin(\Theta/2) \cos(\Theta/2)$$

$$- 8\pi \frac{\sin(\Theta/2)}{\cos(\Theta/2)} \ln(\sin(\Theta/2)), \qquad (55)$$
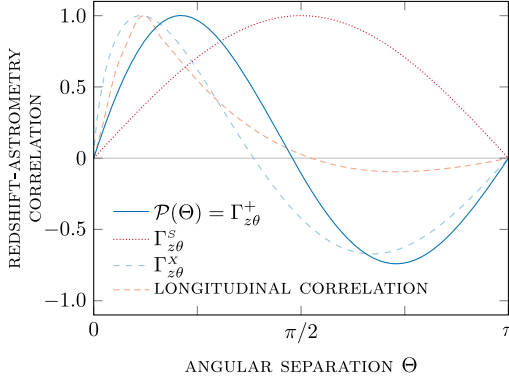
FIG. 12. The redshift-astrometric correlations as a function of angular separation on the sky, given by Eqs. (53), (55), and (56) for different polarizations. The numerical result for the scalar longitudinal correlation is plotted too (see Appendix F 1). All functions are normalized so that their maximum is unity.

$$\Gamma_{z\theta}^X(\Theta) = \frac{2\pi}{3} \sin(\Theta/2) \cos(\Theta/2), \qquad (56)$$

while the correlations $\Gamma_{z\phi}^S$, $\Gamma_{z\phi}^X$, $\Gamma_{z\theta}^Y$ and $\Gamma_{z\phi}^Y$ all vanish. The scalar longitudinal mode curve cannot be derived explicitly using this method, and has therefore been computed numerically (again, only the $x - \theta$ correlation is nonzero). Plots of all four curves can be found in Fig. 12.

Again, the redshift-astrometric correlation pattern is fully described by a single real-valued function of the angular separation, $\mathcal{P}(\Theta)$. This is the redshift-astrometric analog of the Hellings-Downs curve, and is a similarly robust prediction within GR. The three functions $\mathcal{H}(\Theta)$, $\mathcal{T}(\Theta)$ and $\mathcal{P}(\Theta)$ provide a starting point for searching for a stochastic GW background using a combination of pulsar timing and astrometric data; $\mathcal{H}(\Theta)$ describes the spatial correlations of the redshift over the sky, $\mathcal{T}(\Theta)$ describes the astrometric correlations, and $\mathcal{P}(\Theta)$ describes the cross correlation between the redshifts and astrometric deflections.

VI. CONCLUSIONS

The change in the apparent position of a star, or the astrometric response, caused by an arbitrarily polarized gravitational wave has been considered. This astrometric response depends, in general, on both the metric perturbation at the photon emission and absorption events at the star and Earth respectively. If the star is many gravitational wavelengths distant from the Earth, and if the GW is transverse (i.e., $+$, $\times$, and S), then the star terms can be neglected and the astrometric deflection depends only on the metric perturbation near the Earth.

This paper considered the correlated astrometric signal due to a stationary and isotropic GW background. If the background is unpolarized, then the correlation separates into a sum of an integral over the sphere of the sky for each polarization state. We evaluated these integrals for each of the six possible GW polarization states, although in one case the integration could only be performed numerically. A new decomposition for the astrometric correlation matrix has been introduced. This decomposition has a clear geometric interpretation and enables a nice comparison with existing results for the redshift correlations from the pulsar timing literature. In the special case of a tensorially polarized GW background, the astrometric correlation is governed by a single function which can be considered as the astrometric analogue of the Hellings-Downs curve.

The cross correlation between the redshift and astrometric signals has also been derived for all six GW polarizations. This may form the basis for a joint pulsar timing and astrometric search for the low-frequency stochastic gravitational wave background.

Future work on this topic should include establishing how the absolute sensitivity of Gaia to stochastic GW backgrounds depends on the polarization content. It would also be possible to consider how the astrometric correlations are changed in the presence of an anisotropic GW background; this would require a more detailed analysis similar to that already performed for redshift correlations [33,40].

The correlation coefficients for the modes of a vector spherical harmonic representation of the astrometric response can also be computed by utilizing the results described here. This was discussed in Ref. [32], albeit in a different formalism, and the results were left in terms of Legendre polynomial projections of an angular power spectra function. Instead, the correlation coefficients can be computed directly by projecting the two-point correlation functions presented in Secs. IV and V onto vector spherical harmonics with $m = \pm 1$ or $m = 0$ for the astrometry correlations and redshift-astrometry corrections respectively. A future work would involve directly computing the correlation coefficients and assessing their detectability by current and future detectors.

Another interesting possibility is to consider how the astrometric and redshift correlations change if the graviton has a mass; the correlations derived in this paper depend on the assumption that GWs propagate at the speed of light.
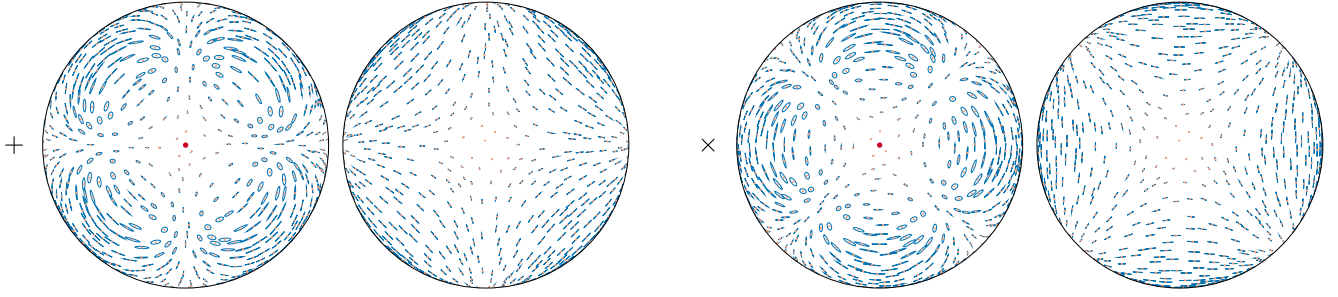
FIG. 13.   Orthographic projections of the Northern (left) and Southern (right) hemispheres. On the sky are chosen 1000 stars. A GW from a source located at the North pole (indicated by the red dots) is incident on the Earth causing the stars to move periodically at the GW frequency, according to Eq. (19). All stars are placed at a distance of 10 gravitational wavelengths from the Earth; in reality, these neat elliptical patterns would appear more chaotic, since the distances to each star are generally different. The blue lines show the resulting movement tracks. The incident GW has the unphysically large characteristic strain amplitude $A = 0.1$.

APPENDIX A: ADDITIONAL ASTROMETRIC DEFLECTION PATTERNS

In Fig. 3 of Sec. III the astrometric deflection patterns were plotted for all six GW polarization states; for the three transverse modes ($+$, $\times$, and S) the distant-source-limit formula (20) was used, while for the three modes with longitudinal components (X, Y, and L) the full formula (including the star terms) (19) was used. In this Appendix the effect of including the star terms on the deflection patterns for the two transverse GR modes ($+$ and $\times$) is illustrated. In Fig. 13 the new astrometric deflection patterns are plotted; these plots were produced in the same way as the top row of Fig. 3 except that Eq. (19) was used in place of Eq. (20) (all stars are placed 10 gravitational wavelengths away from the Earth). The extra terms in the full expression for the astrometric deflection introduce an additional oscillatory deflection pattern which is out of phase with the Earth term pattern plotted in Fig. 3; this causes each star to trace out a small ellipse on the sky. If the stars are further away from the Earth then the phase difference between the two oscillations changes and the amplitude of the additional oscillation is reduced (the ellipses appear rotated and their eccentricity is increased); in the limit of infinite distance the patterns in Fig. 3 are recovered. In these figures the ellipses are aligned in a regular pattern on the sky because the stars are all the same distance from the Earth. If all the distances were different, the ellipses would all be misaligned and the extra motion from the full formula in Eq. (19) would appear to be a random noise superposed on the regular Earth term pattern plotted in Fig. 3.

APPENDIX B: THE TENSORIAL ASTROMETRIC INTEGRALS

In Secs. IV A–IV D the details of the evaluations of the spatial correlation integrals for the different polarization modes were omitted for brevity; the details are presented in this Appendix, and in Appendices D–F.

In the main text the astrometric response at each of the two star positions was resolved in the tangent plane along a pair of basis vectors. It was then shown how the spatial correlation matrix can be written in terms of just two scalar integrals over the sky: one involving the x and θ components, and one involving the y and ϕ components. In this Appendix these two integrals will be evaluated, first for the $+$ mode and then for the $\times$ mode.

First, the $x - \theta$ term for the $+$ polarized GW state is considered; the correlation integral is defined in Eq. (43a) as

$$\Gamma_{x\theta}^+(\Theta) = \int_{S^2} d\Omega_{\mathbf{q}} \delta n_x^+(\mathbf{q}) \delta m_\theta^+(\mathbf{q})$$

$$= \int_0^{2\pi} d\phi \int_0^\pi d\theta \sin\theta \delta n_x^+(\theta, \phi) \delta m_\theta^+(\theta, \phi), \quad \text{(B1)}$$

where the vector $\mathbf{q} = (\sin\theta\cos\phi, \sin\theta\sin\phi, \cos\theta)$ is the direction on the sky from which the GW originates. The components of the astrometric deflections, $\delta n_x^+(\theta, \phi)$ and $\delta m_\theta^+(\theta, \phi)$, may be evaluated from the definitions in Eqs. (41a) and (42a), using the formula for the astrometric deflection in Eq. (20), the expression for the GW basis tensor in Eq. (24a), and the expressions for the basis vectors tangent to the sphere in Eqs. (36a) and (37a):

$$\delta n_x^+(\theta, \phi) = -\frac{1}{2}\sin\theta\cos\phi, \tag{B2a}$$

$$\delta m_\theta^+(\theta, \phi) = \frac{1}{1 - \cos\Theta\cos\theta - \sin\Theta\sin\theta\cos\phi}\left(\frac{3}{16}\sin\Theta(1 - \cos(2\theta)) + \frac{1}{4}(\cos(2\Theta)\sin(2\theta) - 2\cos\Theta\sin\theta)\cos\phi\right.$$

$$\left. + \frac{1}{16}(8\sin\Theta\cos\theta - 3\sin(2\theta) - \sin(2\Theta)\cos(2\theta))\cos(2\phi)\right). \tag{B2b}$$

The azimuthal integral over ϕ in Eq. (B1) may be evaluated using the result derived in Appendix B 1 (previously published in Ref. [40] with a sign error). Using this result the double integral in Eq. (B1) becomes the single integral

$$
\Gamma_{x\theta}^+(\Theta) = -2\pi \int_0^\Theta d\theta (\cos^4(\theta/2) + \cos^2(\theta/2) - 1)\frac{\sin^3(\theta/2)}{\cos(\theta/2)} + 2\pi \int_\Theta^\pi d\theta (\sin^4(\theta/2) + \sin^2(\theta/2) - 1)\frac{\cos^3(\theta/2)}{\sin(\theta/2)}
$$
$$
+ 2\pi \cos^2(\Theta/2) \int_0^\Theta d\theta (2\cos^4(\theta/2) + 1)\frac{\sin^3(\theta/2)}{\cos(\theta/2)} - 2\pi \sin^2(\Theta/2) \int_\Theta^\pi d\theta (2\sin^4(\theta/2) + 1)\frac{\cos^3(\theta/2)}{\sin(\theta/2)}
$$
$$
- \frac{2\pi}{\sin^2(\Theta/2)} \int_0^\Theta d\theta \frac{\sin^5(\theta/2)}{\cos(\theta/2)} + \frac{2\pi}{\cos^2(\Theta/2)} \int_\Theta^\pi d\theta \frac{\cos^5(\theta/2)}{\sin(\theta/2)}. \tag{B3}
$$

This integral may now be evaluated using standard techniques to give

$$
\Gamma_{x\theta}^+(\Theta) = \frac{7\pi}{3} - \frac{14\pi}{3}\sin^2(\Theta/2) - 4\pi\frac{\sin^4(\Theta/2)}{1 - \sin^2(\Theta/2)}
$$
$$
\times \ln(\sin(\Theta/2)) + 4\pi\frac{\cos^4(\Theta/2)}{1 - \cos^2(\Theta/2)}
$$
$$
\times \ln(\cos(\Theta/2)). \tag{B4}
$$

Second, the $y - \phi$ component term for the $+$ polarized GW state is considered; the relevant correlation integral was defined in Eq. (43d) as

$$
\Gamma_{y\phi}^+(\Theta) = \int_0^{2\pi} d\phi \int_0^\pi d\theta \sin\theta \delta n_y^+(\theta, \phi) \delta m_\phi^+(\theta, \phi). \tag{B5}
$$

The components of the astrometric deflections may be evaluated from the definitions in Eqs. (41b) and (42b), using the formula for the astrometric deflection in Eq. (20), the expression for the GW basis tensor in Eq. (24a), and the expressions for the basis vectors in Eqs. (36b) and (37b):

$$
\delta n_y^+(\theta, \phi) = -\frac{1}{2}\sin\theta\sin\phi, \tag{B6a}
$$

$$
\delta m_\phi^+(\theta, \phi) = \frac{1}{1 - \cos\Theta\cos\theta - \sin\Theta\sin\theta\cos\phi}\left(\frac{1}{2}(\cos\Theta\sin\theta\cos\theta - \sin(2\Theta)\sin\theta)\sin\phi \right.
$$
$$
\left. + \frac{1}{8}(2\sin(2\Theta)\cos\theta - 3\sin\Theta - \sin\Theta\cos(2\theta))\sin(2\phi)\right). \tag{B6b}
$$

The integral for $\Gamma_{y\phi}^+(\Theta)$ in Eq. (B5) may be evaluated in the same way as that for $\Gamma_{x\theta}^+(\Theta)$ above to give

$$
\Gamma_{y\phi}^+(\Theta) = -\frac{5\pi}{3} - 4\pi\frac{\sin^4(\Theta/2)}{1 - \sin^2(\Theta/2)}\ln(\sin(\Theta/2))
$$
$$
- 4\pi\frac{\cos^4(\Theta/2)}{1 - \cos^2(\Theta/2)}\ln(\cos(\Theta/2)). \tag{B7}
$$

Third, the two analogous integrals for the $\times$ GR polarization state are considered; these correlation integrals are defined in Eqs. (43a) and (43d):

$$
\Gamma_{x\theta}^\times(\Theta) = \int_0^\pi d\theta \int_0^{2\pi} d\phi \sin\theta \delta n_x^\times(\theta, \phi) \delta m_\theta^\times(\theta, \phi), \tag{B8a}
$$

$$
\Gamma_{y\phi}^\times(\Theta) = \int_0^\pi d\theta \int_0^{2\pi} d\phi \sin\theta \delta n_y^\times(\theta, \phi) \delta m_\phi^\times(\theta, \phi). \tag{B8b}
$$

The components of the astrometric deflection may be evaluated from the definitions in Eqs. (41a), (42a), (41b),

and (42b), using the formula for the astrometric deflection in Eq. (20), the expression for the GW basis tensor in Eq. (24b), and the expressions for the basis vectors in Eqs. (36a), (37a), (36b), and (37b). Due to the symmetry between the $+$ and $\times$ modes, these components are closely related to those found above for the $+$ components:

$$
\delta n_x^\times(\theta, \phi) = \delta n_y^+(\theta, \phi), \tag{B9a}
$$

$$
\delta n_y^\times(\theta, \phi) = -\delta n_x^+(\theta, \phi), \tag{B9b}
$$

$$
\delta m_\theta^\times(\theta, \phi) = \delta m_\phi^+(\theta, \phi), \tag{B9c}
$$

$$
\delta m_\phi^\times(\theta, \phi) = -\delta m_\theta^+(\theta, \phi). \tag{B9d}
$$

The two integrals for $\Gamma_{x\theta}^\times(\Theta)$ and $\Gamma_{y\phi}^\times(\Theta)$ in Eqs. (B8a) and (B8b) may be evaluated in the same way as those for $\Gamma_{x\theta}^+(\Theta)$ and $\Gamma_{y\phi}^+(\Theta)$ above to give

$$
\Gamma_{x\theta}^\times(\Theta) = \Gamma_{y\phi}^+(\Theta), \tag{B10a}
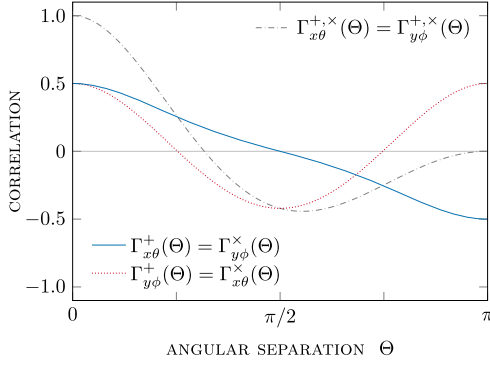$$

FIG. 14. Plot of the tensorial correlation functions in Eq. (B11), normalized so that their absolute maximum is unity. Also shown are the functions for each of the two GR modes, given by Eqs. (B4), (B7), (B10a), and (B10b), rescaled by the same normalization constant.

$$\Gamma_{y\phi}^{\times}(\Theta) = \Gamma_{x\theta}^{+}(\Theta). \qquad (B10b)$$

As was described in the main text, for an unpolarized background containing equal powers of both $+$ and $\times$ polarization states we may define the combined spatial correlation functions $\Gamma_{x\theta}^{+,\times}(\Theta) = \Gamma_{x\theta}^{+}(\Theta) + \Gamma_{x\theta}^{\times}(\Theta)$ and $\Gamma_{y\phi}^{+,\times}(\Theta) = \Gamma_{y\phi}^{+}(\Theta) + \Gamma_{y\phi}^{\times}(\Theta)$. These new functions may be evaluated by taking the sums of the expressions in Eqs. (B4), (B7), (B10a), and (B10b) to give the result which appeared in the main text,

$$\Gamma_{x\theta}^{+,\times}(\Theta) = \Gamma_{y\phi}^{+,\times}(\Theta) = \frac{2\pi}{3} - \frac{14\pi}{3}\sin^2(\Theta/2)$$
$$- 8\pi \frac{\sin^4(\Theta/2)}{1 - \sin^2(\Theta/2)} \ln(\sin(\Theta/2)). \qquad (B11)$$

The three functions $\Gamma_{x\theta}^{+}(\Theta) = \Gamma_{y\phi}^{\times}(\Theta)$, $\Gamma_{y\phi}^{+}(\Theta) = \Gamma_{x\theta}^{\times}(\Theta)$, and $\Gamma_{x\theta}^{+,\times}(\Theta) = \Gamma_{y\phi}^{+,\times}(\Theta)$, are plotted in Fig. 14.

1. Azimuthal integral

The following integral appears in most of the spatial correlation integrals:

$$I_n(\theta, \Theta) = \int_0^{2\pi} d\phi \frac{\cos(n\phi)}{1 - \cos\Theta\cos\theta - \sin\Theta\sin\theta\cos\phi}$$
$$= \Re\left\{\int_0^{2\pi} d\phi \frac{e^{in\phi}}{1 - \cos\Theta\cos\theta - \sin\Theta\sin\theta\cos\phi}\right\}. \qquad (B12)$$

The integral is tidied up by defining the new variables

$$\mathfrak{a}(\theta, \Theta) = 1 - \cos\Theta\cos\theta, \qquad (B13a)$$

$$\mathfrak{b}(\theta, \Theta) = -\frac{\sin\Theta\sin\theta}{1 - \cos\Theta\cos\theta}. \qquad (B13b)$$

If $z = e^{i\phi}$, then $d\phi = dz/(iz)$ and from $\bar{z} = 1/z = \cos\phi - i\sin\phi$, it can be found that $\cos\phi = \frac{1}{2}(z + z^{-1})$ and finally $I_n(\theta, \Theta)$ is expressed as a complex integral over the circle $\gamma = \{|z| = -1/\mathfrak{b}\}$

$$I_n(\theta, \Theta) = \Re\left\{\frac{2}{i\mathfrak{a}} \oint_\gamma dz \frac{z^{|n|}}{\mathfrak{b}z^2 + 2z + \mathfrak{b}}\right\}. \qquad (B14)$$

The modulus sign is needed since the cosine function is even. The integrand has two distinct poles, each at $z_\pm = (-1 \pm \sqrt{1 - \mathfrak{b}^2})/\mathfrak{b}$. The positions of those poles are determined by the range of the function $\mathfrak{b}(\theta, \Theta)$. Both θ and Θ range from 0 to π; the substitutions $x = \cos\theta$ and $y = \cos\Theta$ lead to

$$\mathfrak{b}(x, y) = -\frac{\sqrt{1 - x^2}\sqrt{1 - y^2}}{1 - xy}. \qquad (B15)$$

By investigating the derivatives of $\mathfrak{b}(x, y)$, it can be established that the function ranges between -1 and 0, which corresponds to $z_- \in [-1/\mathfrak{b}, +\infty)$ and $z_+ \in (0, -1/\mathfrak{b}]$. The value of the contour integral is determined by the residue of the root which lies inside the contour γ,

$$2\pi i \Res_{z=z_+}\left\{\frac{z^n}{\mathfrak{b}z^2 + 2z + \mathfrak{b}}\right\} = \pi i \frac{z_+^n}{\mathfrak{b}z_+ + 1}. \qquad (B16)$$

Plugging this back into Eq. (B14) yields a result for I_n,

$$I_n(\theta, \Theta) = \frac{2\pi}{\mathfrak{a}\sqrt{1 - \mathfrak{b}^2}}\left(\frac{-1 + \sqrt{1 - \mathfrak{b}^2}}{\mathfrak{b}}\right)^{|n|}$$
$$= \frac{2\pi}{|\cos\theta - \cos\Theta|}$$
$$\times \left(\frac{1 - \cos\Theta\cos\theta + |\cos\theta - \cos\Theta|}{\sin\Theta\sin\theta}\right)^{|n|}$$
$$\qquad (B17a)$$

$$= \begin{cases} \frac{2\pi}{\cos\theta - \cos\Theta}\left(\frac{(1+\cos\Theta)(1-\cos\theta)}{(1-\cos\Theta)(1+\cos\theta)}\right)^{|n|/2}, & 0 \leq \theta \leq \Theta, \\ \frac{2\pi}{\cos\Theta - \cos\theta}\left(\frac{(1-\cos\Theta)(1+\cos\theta)}{(1+\cos\Theta)(1-\cos\theta)}\right)^{|n|/2}, & \Theta < \theta \leq \pi. \end{cases}$$
$$\qquad (B17b)$$

APPENDIX C: RANDOM REALIZATIONS OF THE ASTROMETRIC DEFLECTIONS ON THE SKY

Figures 6 and 8 show one possible realization of the GW background for the GR and transverse scalar polarizations respectively. In this Appendix the method for producing such realizations is described.

Pick N distinct arbitrary points (or "stars") on the sky. The Cartesian coordinates of the ith star are $\mathbf{n}_i = (x_i, y_i, z_i)$

and satisfy $x_i^2 + y_i^2 + z_i^2 = 1$. Consider the following vector of length $3N$ formed from the Cartesian coordinates:

$$\mathbf{x} = (x_1, y_1, z_1, x_2, y_2, z_2, \ldots, x_N, y_N, z_N). \quad (C1)$$

The quantity one needs to find is the change in these coordinates, $\delta\mathbf{x}$. Formally, this is distributed as a zero-mean Gaussian random variable,

$$\delta\mathbf{x} \sim \mathcal{N}(\mathbf{0}, \mathbf{C}), \quad (C2)$$

with the $3N \times 3N$ correlation matrix formed block by block from the 3×3 spatial matrices defined in Eq. (32):

$$\mathbf{C} = \begin{pmatrix} \mathbf{\Gamma}(\mathbf{n}_1, \mathbf{n}_1) & \mathbf{\Gamma}(\mathbf{n}_1, \mathbf{n}_2) & \cdots & \mathbf{\Gamma}(\mathbf{n}_1, \mathbf{n}_N) \\ \mathbf{\Gamma}(\mathbf{n}_2, \mathbf{n}_1) & \mathbf{\Gamma}(\mathbf{n}_2, \mathbf{n}_2) & \cdots & \mathbf{\Gamma}(\mathbf{n}_2, \mathbf{n}_N) \\ \vdots & \vdots & \ddots & \vdots \\ \mathbf{\Gamma}(\mathbf{n}_N, \mathbf{n}_1) & \mathbf{\Gamma}(\mathbf{n}_N, \mathbf{n}_2) & \cdots & \mathbf{\Gamma}(\mathbf{n}_N, \mathbf{n}_N) \end{pmatrix}. \quad (C3)$$

This is only valid formally, because the matrix $\mathbf{C}$ is not positive definite; in fact, it has N zero eigenvalues. The origin of this behavior is that the three Cartesian coordinates are being used to describe an intrinsically two-dimensional process on the sphere. This can be rectified by instead considering the changes in the polar coordinates of each star:

$$\begin{pmatrix} \delta\theta_i \\ \delta\phi_i \end{pmatrix} = \mathbf{P}_i \cdot \begin{pmatrix} \delta x_i \\ \delta y_i \\ \delta z_i \end{pmatrix},$$

where $\mathbf{P}_i = \begin{pmatrix} 0 & 0 & -\frac{1}{\sqrt{1-z_i^2}} \\ -\frac{y_i}{x_i^2+y_i^2} & \frac{x_i}{x_i^2+y_i^2} & 0 \end{pmatrix} \quad (C4)$

$$\Rightarrow \boldsymbol{\delta\theta} \equiv (\delta\theta_1, \delta\phi_1, \delta\theta_2, \delta\phi_2, \ldots, \delta\theta_N, \delta\phi_N)$$

$$= \mathbf{\Pi} \cdot \boldsymbol{\delta\mathbf{x}}$$

where $\mathbf{\Pi} = \begin{pmatrix} \mathbf{P}_1 & \mathbf{0} & \cdots & \mathbf{0} \\ \mathbf{0} & \mathbf{P}_2 & \cdots & \mathbf{0} \\ \vdots & \vdots & \ddots & \vdots \\ \mathbf{0} & \mathbf{0} & \cdots & \mathbf{P}_N \end{pmatrix}. \quad (C5)$

The matrix $\mathbf{\Pi}$ has shape $2N \times 3N$. The vector $\boldsymbol{\delta\theta}$ is also distributed as a Gaussian random variable, $\boldsymbol{\delta\theta} \sim \mathcal{N}(\mathbf{0}, \mathbf{C}')$, where the new covariance matrix $\mathbf{C}' = \mathbf{\Pi} \cdot \mathbf{C} \cdot \mathbf{\Pi}^{\mathrm{T}}$ is strictly positive definite. The parameter A is some overall amplitude chosen in Figs. 6 and 8 to be $A = 0.01$. A random realization of $\boldsymbol{\delta\theta}$ may now be obtained without an obstacle, and the vector $\boldsymbol{\delta\mathbf{x}}$ can be obtained by simple geometry.

The plots in Figs. 6 and 8 were produced using $N = 1000$ stars placed regularly on the sky, and show the original star positions, $\mathbf{x}$, and the new positions, $\mathbf{x} + \boldsymbol{\delta\mathbf{x}}$, joined by a smooth curves using the Mollweide projection.

APPENDIX D: THE TRANSVERSE SCALAR "BREATHING" MODE ASTROMETRIC INTEGRALS

In this Appendix the evaluation of spatial correlation integrals for the transverse scalar GW polarization state, S, is briefly described. The integration is very similar to those for the $+$ and $\times$ states described in Appendix B. The relevant correlation integrals were defined in Eqs. (43a) and (43d) as

$$\Gamma_{x\theta}^S(\Theta) = \int_{S^2} d\Omega_{\mathbf{q}} \delta n_x^S(\mathbf{q}) \delta m_\theta^S(\mathbf{q})$$

$$= \int_0^{2\pi} d\phi \int_0^\pi d\theta \sin\theta \delta n_x^S(\theta, \phi) \delta m_\theta^S(\theta, \phi), \quad (D1a)$$

$$\Gamma_{y\phi}^S(\Theta) = \int_{S^2} d\Omega_q \delta n_y^S(\mathbf{q}) \delta m_\phi^S(\mathbf{q})$$

$$= \int_0^{2\pi} d\phi \int_0^\pi d\theta \sin\theta \delta n_y^S(\theta, \phi) \delta m_\phi^S(\theta, \phi), \quad (D1b)$$

where the vector $\mathbf{q} = (\sin\theta\cos\phi, \sin\theta\sin\phi, \cos\theta)$ is the direction on the sky from which the GW originates. The components of the astrometric deflections may be evaluated from the definitions in Eqs. (41a), (42a), (41b), and (42b), using the formula for the astrometric deflection in Eq. (20), the expression for the GW basis tensor in Eq. (24c), and the expressions for the basis vectors tangent to the sphere in Eqs. (36a), (37a), (36b), and (37b):

$$\delta n_x^S(\theta, \phi) = -\frac{1}{2}\sin\theta\cos\phi, \quad (D2a)$$

$$\delta n_y^S(\theta, \phi) = \delta m_\phi^S(\theta, \phi) = -\frac{1}{2}\sin\theta\sin\phi, \quad (D2b)$$

$$\delta m_\theta^S(\theta, \phi) = \frac{1}{2}\sin\Theta\cos\theta - \frac{1}{2}\cos\Theta\sin\theta\cos\phi. \quad (D2c)$$

The azimuthal and polar integrals for $\Gamma_{x\theta}^S(\Theta)$ and $\Gamma_{y\phi}^S(\Theta)$ in Eqs. (D1a) and (D1b) may be evaluated in the same way as those for $\Gamma_{x\theta}^{+,\times}(\Theta)$ and $\Gamma_{y\phi}^{+,\times}(\Theta)$ in Appendix B to give the results in Eqs. (47a) and (47b) of the main text.

APPENDIX E: THE VECTORIAL ASTROMETRIC INTEGRALS

In this Appendix the evaluation of spatial correlation integrals for the vectorial GW polarization states, X and Y, is briefly described. The derivation is very similar to those for the $+$ and $\times$ states described in Appendix B. What is

interesting in this case is that even though the stand-alone astrometric response in both vectorial polarizations is divergent at the origin (in Fig. 3 the "star terms" were added to remove this divergence), the correlation functions are perfectly regular and finite for all relevant values of Θ.

First, the X mode is considered; the relevant correlation integrals were defined in Eqs. (43a) and (43d) as

$$
\begin{aligned}
\Gamma_{x\theta}^{X}(\Theta) &= \int_{S^2} d\Omega_{\mathbf{q}} \delta n_x^X(\mathbf{q}) \delta m_\theta^X(\mathbf{q}) \\
&= \int_0^{2\pi} d\phi \int_0^\pi d\theta \sin\theta \delta n_x^X(\theta,\phi) \delta m_\theta^X(\theta,\phi),
\end{aligned} \quad \text{(E1a)}
$$

$$
\begin{aligned}
\Gamma_{y\phi}^{X}(\Theta) &= \int_{S^2} d\Omega_{\mathbf{q}} \delta n_y^X(\mathbf{q}) \delta m_\phi^X(\mathbf{q}) \\
&= \int_0^{2\pi} d\phi \int_0^\pi d\theta \sin\theta \delta n_y^X(\theta,\phi) \delta m_\phi^X(\theta,\phi),
\end{aligned} \quad \text{(E1b)}
$$

where the vector $\mathbf{q} = (\sin\theta\cos\phi, \sin\theta\sin\phi, \cos\theta)$ is the direction on the sky from which the GW originates. The components of the astrometric deflections may be evaluated from the definitions in Eqs. (41a), (42a), (41b), and (42b), using the formula for the astrometric deflection in Eq. (20), the expression for the GW basis tensor in Eq. (24d), and the expressions for the basis vectors tangent to the sphere in Eqs. (36a), (37a), (36b), and (37b):

$$
\delta n_x^X(\theta,\phi) = \frac{1}{2}(1 + 2\cos\theta)\cos\phi, \quad \text{(E2a)}
$$

$$
\delta n_y^X(\theta,\phi) = \frac{1}{2}(1 + 2\cos\theta)\sin\phi, \quad \text{(E2b)}
$$

$$
\begin{aligned}
\delta m_\theta^X(\theta,\phi) = &\frac{1}{1 - \cos\Theta\cos\theta - \sin\Theta\sin\theta\cos\phi} \\
&\times \Bigg(\frac{1}{8}(2\sin\Theta\sin\theta - 3\sin(2\Theta)\sin(2\theta)) \\
&+ \frac{1}{2}(\cos\Theta\cos\theta - \cos(2\Theta)\cos(2\theta))\cos\phi \\
&+ \frac{1}{4}(\sin\Theta\sin\theta - \sin(2\Theta)\sin(2\theta))\cos(2\phi) \Bigg),
\end{aligned}
$$
$$\text{(E2c)}$$

$$
\begin{aligned}
\delta m_\phi^X(\theta,\phi) = &\frac{1}{1 - \cos\Theta\cos\theta - \sin\Theta\sin\theta\cos\phi} \\
&\times \Bigg(\frac{1}{2}\cos\Theta(\cos\theta - \cos(2\theta))\sin\phi \\
&+ \frac{1}{4}(\sin(2\Theta)\sin\theta - \sin\Theta\sin(2\theta))\sin(2\phi) \Bigg).
\end{aligned}
$$
$$\text{(E2d)}$$

The equations for $\delta m_\theta^X(\theta,\phi)$ and $\delta m_\phi^X(\theta,\phi)$ diverge when $\Theta = 0$. Nevertheless, the azimuthal and polar integrals for

$\Gamma_{y\phi}^X(\Theta)$ and $\Gamma_{y\phi}^X(\Theta)$ in Eqs. (E1a) and (E1b) may be evaluated in the same way as those for $\Gamma_{x\theta}^{+,\times}(\Theta)$ and $\Gamma_{y\phi}^{+,\times}(\Theta)$ in Appendix B to give two results that are regular for all values of Θ:

$$
\begin{aligned}
\Gamma_{x\theta}^{X}(\Theta) = &\frac{\pi}{6} + \frac{2\pi}{3}\sin^2(\Theta/2) + 6\pi\frac{\sin^2(\Theta/2)}{1 - \sin^2(\Theta/2)} \\
&\times \ln(\sin(\Theta/2)) - 2\pi\frac{\cos^2(\Theta/2)}{1 - \cos^2(\Theta/2)} \\
&\times \ln(\cos(\Theta/2)),
\end{aligned} \quad \text{(E3a)}
$$

$$
\begin{aligned}
\Gamma_{y\phi}^{X}(\Theta) = &\frac{13\pi}{6} + \pi\sin^2(\Theta/2) + 6\pi\frac{\sin^2(\Theta/2)}{1 - \sin^2(\Theta/2)} \\
&\times \ln(\sin(\Theta/2)) + 2\pi\frac{\cos^2(\Theta/2)}{1 - \cos^2(\Theta/2)} \\
&\times \ln(\cos(\Theta/2)).
\end{aligned} \quad \text{(E3b)}
$$

Second, the Y mode is considered; the relevant correlation integrals were defined in Eqs. (43a) and (43d) as

$$
\Gamma_{x\theta}^{Y}(\Theta) = \int_0^{2\pi} d\phi \int_0^\pi d\theta \sin\theta \delta n_x^Y(\theta,\phi) \delta m_\theta^X(\theta,\phi), \quad \text{(E4a)}
$$

$$
\Gamma_{y\phi}^{Y}(\Theta) = \int_0^{2\pi} d\phi \int_0^\pi d\theta \sin\theta \delta n_y^Y(\theta,\phi) \delta m_\phi^X(\theta,\phi). \quad \text{(E4b)}
$$

The components of the astrometric deflections may be evaluated from the definitions in Eqs. (41a), (42a), (41b), and (42b), using the formula for the astrometric deflection in Eq. (20), the expression for the GW basis tensor in Eq. (24e), and the expressions for the basis vectors tangent to the sphere in Eqs. (36a), (37a), (36b), and (37b):

$$
\delta n_x^Y(\theta,\phi) = \frac{1}{2}\cos\theta\sin\phi, \quad \text{(E5a)}
$$

$$
\delta n_y^Y(\theta,\phi) = -\frac{1}{2}\cos\theta\cos\phi, \quad \text{(E5b)}
$$

$$
\begin{aligned}
\delta m_\theta^Y(\theta,\phi) = &\frac{1}{1 - \cos\Theta\cos\theta - \sin\Theta\sin\theta\cos\phi} \\
&\times \Bigg(\frac{1}{2}(\cos(2\Theta) - \cos\Theta\cos\theta)\cos\theta\sin\phi \\
&+ \frac{1}{4}\sin\Theta(2\cos\Theta - \cos\theta)\sin\theta\sin(2\phi) \Bigg),
\end{aligned}
$$
$$\text{(E5c)}$$

$$
\begin{aligned}
\delta m_\phi^Y(\theta,\phi) = &\frac{1}{1 - \cos\Theta\cos\theta - \sin\Theta\sin\theta\cos\phi} \\
&\times \Bigg(\frac{3}{16}\sin(2\Theta)\sin(2\theta) + \frac{1}{4}(1 - 2\cos\Theta\cos\theta \\
&+ \cos(2\Theta)\cos(2\theta))\cos\phi + \frac{1}{16}(\sin(2\Theta)\sin(2\theta) \\
&- 8\sin\Theta\sin\theta)\cos(2\phi) \Bigg).
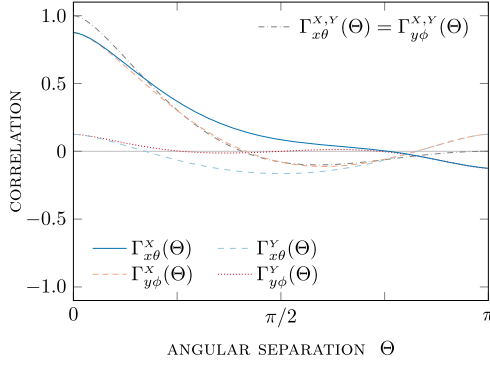\end{aligned}
$$
$$\text{(E5d)}$$

FIG. 15. Plot of the vectorial correlation functions in Eq. (50), normalized so that their absolute maximum is unity. Also shown are the functions for each of the two GR modes, given by Eqs. (E3a), (E3b), (E6a), and (E6b), rescaled by the same normalization constant.

The integrals for $\Gamma_{y\phi}^{Y}(\Theta)$ and $\Gamma_{y\phi}^{Y}(\Theta)$ in Eqs. (E4a) and (E4b) may be evaluated in the same way as the integrals in Appendix B:

$$\Gamma_{x\theta}^{Y}(\Theta) = \frac{7\pi}{6} + 2\pi \frac{\sin^2(\Theta/2)}{1 - \sin^2(\Theta/2)} \ln(\sin(\Theta/2))$$

$$+ 2\pi \frac{\cos^2(\Theta/2)}{1 - \cos^2(\Theta/2)} \ln(\cos(\Theta/2)), \quad \text{(E6a)}$$

$$\Gamma_{y\phi}^{Y}(\Theta) = -\frac{5\pi}{6} + \frac{5\pi}{3}\sin^2(\Theta/2) + 2\pi \frac{\sin^2(\Theta/2)}{1 - \sin^2(\Theta/2)}$$

$$\times \ln(\sin(\Theta/2)) - 2\pi \frac{\cos^2(\Theta/2)}{1 - \cos^2(\Theta/2)}$$

$$\times \ln(\cos(\Theta/2)). \quad \text{(E6b)}$$

As was described in the main text, for a unpolarized background containing equal powers of both X and Y polarization states we may define the combined spatial correlation functions $\Gamma_{x\theta}^{X,Y}(\Theta) = \Gamma_{x\theta}(\Theta)^X + \Gamma_{x\theta}^{Y}(\Theta)$ and $\Gamma_{y\phi}(\Theta)^{X,Y} = \Gamma_{y\phi}(\Theta)^X + \Gamma_{y\phi}^{Y}(\Theta)$. These new functions may be evaluated by taking the sums of the expressions in Eqs. (E3a), (E3b), (E6a), and (E6b) to give the results which appeared in Eq. (50) of the main text.

The functions $\Gamma_{x\theta}^{X}(\Theta)$, $\Gamma_{y\phi}^{X}(\Theta)$, $\Gamma_{y\phi}^{Y}(\Theta)$, $\Gamma_{x\theta}^{Y}(\Theta)$, and $\Gamma_{x\theta}^{X,Y}(\Theta) = \Gamma_{y\phi}^{X,Y}(\Theta)$, are plotted in Fig. 15.

APPENDIX F: THE SCALAR LONGITUDINAL ASTROMETRIC INTEGRALS

In this Appendix the evaluation of spatial correlation integrals for the longitudinal scalar GW polarization state, L, will be discussed. Using the method established in the previous appendices will yield divergent curves. These results are still useful, and reasons for the anomaly are discussed in Sec. IV D. A more careful calculation which

removes the divergence is presented in Appendix F 1. The integration is very similar to those for the + and × states described in Appendix B. The relevant correlation integrals were defined in Eqs. (43a) and (43d) as

$$\Gamma_{x\theta}^{L}(\Theta) = \int_{S^2} d\Omega_q \delta n_x^{L}(\mathbf{q}) \delta m_\theta^{L}(\mathbf{q})$$

$$= \int_0^{2\pi} d\phi \int_0^{\pi} d\theta \sin\theta \delta n_x^{L}(\theta, \phi) \delta m_\theta^{L}(\theta, \phi), \quad \text{(F1a)}$$

$$\Gamma_{y\phi}^{L}(\Theta) = \int_{S^2} d\Omega_q \delta n_y^{L}(\mathbf{q}) \delta m_\phi^{L}(\mathbf{q})$$

$$= \int_0^{2\pi} d\phi \int_0^{\pi} d\theta \sin\theta \delta n_y^{L}(\theta, \phi) \delta m_\phi^{L}(\theta, \phi), \quad \text{(F1b)}$$

where the vector $\mathbf{q} = (\sin\theta\cos\phi, \sin\theta\sin\phi, \cos\theta)$ is the direction on the sky from which the GW originates. The components of the astrometric deflections may be evaluated from the definitions in Eqs. (41a), (42a), (41b), and (42b), using the formula for the astrometric deflection in Eq. (20), the expression for the GW basis tensor in Eq. (24f), and the expressions for the basis vectors tangent to the sphere in Eqs. (36a), (37a), (36b), and (37b):

$$\delta n_x^{L} = -\frac{1}{\sqrt{2}} \frac{\sin\theta\cos\theta\cos\phi}{1 - \cos\theta}, \quad \text{(F2a)}$$

$$\delta n_y^{L} = -\frac{1}{\sqrt{2}} \frac{\sin\theta\cos\theta\sin\phi}{1 - \cos\theta}, \quad \text{(F2b)}$$

$$\delta m_\theta^{L} = \frac{1}{\sqrt{2}(1 - \cos\Theta\cos\theta - \sin\Theta\sin\theta\cos\phi)}$$

$$\times \left(\frac{1}{8}\sin(2\Theta)(1 + 3\cos(2\theta)) \right.$$

$$+ \frac{1}{4}\cos(2\Theta)\sin(2\theta)\cos\phi$$

$$\left. + \frac{1}{8}\sin(2\Theta)(\cos(2\theta) - 1)\cos(2\phi) \right), \quad \text{(F2c)}$$

$$\delta m_\phi^{L} = \frac{1}{\sqrt{2}(1 - \cos\Theta\cos\theta - \sin\Theta\sin\theta\cos\phi)}$$

$$\times \left(\frac{1}{2}\cos\Theta\sin(2\theta)\sin\phi \right.$$

$$\left. + \frac{1}{4}\sin\Theta(1 - \cos(2\theta))\sin(2\phi) \right). \quad \text{(F2d)}$$

The integrals for $\Gamma_{y\phi}^{L}(\Theta)$ and $\Gamma_{y\phi}^{L}(\Theta)$ in Eqs. (F1a) and (F1b) may be evaluated in the same way as those for $\Gamma_{x\theta}^{+,\times}(\Theta)$ and $\Gamma_{y\phi}^{+,\times}(\Theta)$ in Appendix B to give the results presented in Sec. IV D of the main text (51a) and (51b).

As evident from Fig. 10, where these two curves are plotted, they diverge at $\Theta = 0$. Obviously, this implies that in the context of the scalar longitudinal mode, the method for calculating the overlap reduction function is

inapplicable. We present below a modified approach which solves the issue of the divergent curves.

1. Numerical correlation integrals on the sphere

The cause of the divergence in Eqs. (51a) and (51b) is the use of the distant-source version of the astrometric

$$
\begin{aligned}
\Delta_{i}{}^{jk}(\mathbf{n}, \mathbf{q}, d) = \Bigg(& \left\{ 1 + \frac{i(2 - q^r n_r)}{d(1 - q^\ell n_\ell)} \left(1 - \exp\left(-id(1 - q^s n_s) \right) \right) \right\} n_{\hat{\imath}} \\
& - \left\{ 1 + \frac{i}{d(1 - q^\ell n_\ell)} \left(1 - \exp\left(-id(1 - q^s n_s) \right) \right) \right\} q_{\hat{\imath}} \Bigg) \frac{n^j n^k}{2(1 - q^\ell n_\ell)} \\
& - \left\{ \frac{1}{2} + \frac{i}{d(1 - q^\ell n_\ell)} \left(1 - \exp\left(-id(1 - q^s n_s) \right) \right) \right\} \delta_i{}^j n^k,
\end{aligned}
\tag{F3}
$$

where $d = \omega \lambda_S \Omega$ is a measure of the distance to the star (in gravitational wavelengths). With this form of $\Delta_i{}^{jk}$, the integral becomes regular for all relevant values of Θ. The correlation curve is now a three-parameter function of the angle on the sky Θ and the distances to both stars, d_n and d_m:

$$
\begin{aligned}
\Gamma^L_{x\theta}(\Theta, d_n, d_m) &= \int_{S^2} d\Omega_\mathbf{q} \, \delta n^L_x(\mathbf{q}, d_n) \delta m^L_\theta(\mathbf{q}, d_m) \\
&= \int_0^{2\pi} d\phi \int_0^{\pi} d\theta \sin\theta \, \delta n^L_x(\theta, \phi, d_n) \\
&\quad \times \delta m^L_\theta(\theta, \phi, d_m),
\end{aligned}
\tag{F4a}
$$

$$
\begin{aligned}
\Gamma^L_{y\phi}(\Theta, d_n, d_m) &= \int_{S^2} d\Omega_\mathbf{q} \, \delta n^L_y(\mathbf{q}, d_n) \delta m^L_\phi(\mathbf{q}, d_m) \\
&= \int_0^{2\pi} d\phi \int_0^{\pi} d\theta \sin\theta \, \delta n^L_y(\theta, \phi, d_n) \\
&\quad \times \delta m^L_\phi(\theta, \phi, d_m).
\end{aligned}
\tag{F4b}
$$

The vector $\mathbf{q} = (\sin\theta \cos\phi, \sin\theta \sin\phi, \cos\theta)$ is the direction on the sky from which the GW originates. The components of the astrometric deflections may be evaluated from the definitions in Eqs. (41a), (42a), (41b), and (42b), using the formula for the astrometric deflection in Eq. (19), the expression for the GW basis tensor in Eq. (24f), and the expressions for the basis vectors tangent to the sphere in Eqs. (36a), (37a), (36b), and (37b). Unfortunately, the integrals in Eqs. (F4a) and (F4b) can no longer be solved using the same method as above, and need to be evaluated numerically. Let $\mathcal{L}_{x\theta}(\Theta)$ be the result of numerically evaluating $\Gamma^L_{x\theta}(\Theta)$ and $\mathcal{L}_{y\phi}(\Theta)$ be the result

response in Eq. (20). If the full astrometric response in Eq. (51a) is used instead the resulting spatial correlation is always finite (although no longer analytically tractable). All of the general discussion of the spatial correlation in Sec. IV proceeds exactly as before, except Eq. (29) now becomes the distance-dependent expression

of numerically evaluating $\Gamma^L_{y\phi}(\Theta)$. In Fig. 10 two curves $\mathcal{L}_{x\theta}(\Theta)$ and $\mathcal{L}_{y\phi}(\Theta)$ are shown as examples of these integrals for $(d_n, d_m) = (100, 200)$. It becomes evident that the numerical curves tend to the two analytic functions (51a) and (51b) for large Θ.

2. Correlation integrals for stars in the same direction on the sky

The integrals (F4a) and (F4b) can be solved analytically for the case $\Theta = 0$ (and also for $\Theta = \pi$) to give a two-parameter family of functions which quantifies the correlation between the astrometric deflections of stars with the same position on the sky but located at different distances,

$$
\begin{aligned}
\Sigma^L & (d_\mathbf{n}, d_\mathbf{m}) \\
&= \int_0^{2\pi} d\phi \int_0^{\pi} d\theta \sin\theta \, \delta n^L_x(d_\mathbf{n}, \theta, \phi) \delta m^L_\theta(d_\mathbf{m}, \theta, \phi) \Bigg|_{\Theta=0} \\
&= \int_0^{2\pi} d\phi \int_0^{\pi} d\theta \sin\theta \, \delta n^L_x(d_\mathbf{n}, \theta, \phi) \delta n^L_x(d_\mathbf{m}, \theta, \phi).
\end{aligned}
\tag{F5}
$$

The derivation involves a simple azimuthal integral which yields another straightforward polar integral. The components of the astrometric deflections (at $\Theta = 0$) may be evaluated from the definitions in Eqs. (41a), (42a), (41b), and (42b), using the formula for the astrometric deflection in Eq. (19), the expression for the GW basis tensor in Eq. (24f), and the expressions for the basis vectors tangent to the sphere in Eqs. (36a), (37a), (36b), and (37b):

$$\delta n_x^L(d,\theta,\phi) = \delta n_y^L(d,\theta,\phi) = -\frac{1}{\sqrt{2}}\left(\frac{\cos^3(\theta/2)}{\sin(\theta/2)} - \sin(\theta/2)\cos(\theta/2)\right)\cos\phi$$
$$+\frac{1}{2\sqrt{2}d}(3-2\cos^2(\theta/2))\left(\frac{\cos^3(\theta/2)}{\sin^3(\theta/2)} - \frac{\cos(\theta/2)}{\sin(\theta/2)}\right)\sin(2d\sin^2(\theta/2))\cos\phi. \tag{F6}$$

The integral for $\Sigma^L(d_{\mathbf{n}},d_{\mathbf{m}})$ in Eq. (F5) may be evaluated using a computer algebra package to give

$$\Sigma^L(d_{\mathbf{n}},d_{\mathbf{m}}) = \pi\gamma + \pi\ln(2) - \frac{29\pi}{30} + \frac{33\pi}{d_{\mathbf{n}}^4} + \frac{33\pi}{d_{\mathbf{m}}^4} + \frac{11\pi}{2d_{\mathbf{n}}^2} + \frac{11\pi}{2d_{\mathbf{m}}^2} - \frac{90\pi}{(d_{\mathbf{n}}^2-d_{\mathbf{m}}^2)^2} + \pi\ln(d_{\mathbf{n}}d_{\mathbf{m}})$$
$$-\pi\frac{(d_{\mathbf{n}}+d_{\mathbf{m}}-2)(d_{\mathbf{n}}+d_{\mathbf{m}}+2)}{4d_{\mathbf{n}}d_{\mathbf{m}}}\ln(d_{\mathbf{n}}+d_{\mathbf{m}}) + \pi\frac{(d_{\mathbf{n}}-d_{\mathbf{m}}-2)(d_{\mathbf{n}}-d_{\mathbf{m}}+2)}{4d_{\mathbf{n}}d_{\mathbf{m}}}\ln|d_{\mathbf{n}}-d_{\mathbf{m}}|$$
$$-\pi\mathrm{Ci}(2d_{\mathbf{n}}) - \pi\mathrm{Ci}(2d_{\mathbf{m}}) - \frac{9\pi}{2d_{\mathbf{n}}}\mathrm{Si}(2d_{\mathbf{n}}) - \frac{9\pi}{2d_{\mathbf{m}}}\mathrm{Si}(2d_{\mathbf{m}})$$
$$+\pi\frac{(d_{\mathbf{n}}+d_{\mathbf{m}}-2)(d_{\mathbf{n}}+d_{\mathbf{m}}+2)}{4d_{\mathbf{n}}d_{\mathbf{m}}}\mathrm{Ci}(2(d_{\mathbf{n}}+d_{\mathbf{m}})) - \pi\frac{(d_{\mathbf{n}}-d_{\mathbf{m}}-2)(d_{\mathbf{n}}+d_{\mathbf{m}}+2)}{4d_{\mathbf{n}}d_{\mathbf{m}}}\mathrm{Ci}(2|d_{\mathbf{n}}-d_{\mathbf{m}}|)$$
$$+\frac{15\pi(d_{\mathbf{n}}+d_{\mathbf{m}})}{4d_{\mathbf{n}}d_{\mathbf{m}}}\mathrm{Si}(2(d_{\mathbf{n}}+d_{\mathbf{m}})) - \frac{15\pi(d_{\mathbf{n}}-d_{\mathbf{m}})}{4d_{\mathbf{n}}d_{\mathbf{m}}}\mathrm{Si}(2|d_{\mathbf{n}}-d_{\mathbf{m}}|))$$
$$-\pi\frac{5d_{\mathbf{n}}^2-54}{2d_{\mathbf{n}}^4}\cos(2d_{\mathbf{n}}) - \pi\frac{5d_{\mathbf{m}}^2-54}{2d_{\mathbf{m}}^4}\cos(2d_{\mathbf{m}}) + \pi\frac{d_{\mathbf{n}}^4+11d_{\mathbf{n}}^2-60}{2d_{\mathbf{n}}^5}\sin(2d_{\mathbf{n}}) + \pi\frac{d_{\mathbf{m}}^4+11d_{\mathbf{m}}^2-60}{2d_{\mathbf{m}}^5}\sin(2d_{\mathbf{m}})$$
$$-\frac{10\pi}{(d_{\mathbf{n}}^2-d_{\mathbf{m}}^2)^2}\cos(2d_{\mathbf{n}})\cos(2d_{\mathbf{m}}) - \pi\frac{(d_{\mathbf{n}}^2-d_{\mathbf{m}}^2)^3 - 12(d_{\mathbf{n}}^2-d_{\mathbf{m}}^2)^2 + 100(d_{\mathbf{n}}^2+3d_{\mathbf{m}}^2)}{4(d_{\mathbf{n}}^2-d_{\mathbf{m}}^2)^3 d_{\mathbf{m}}}\cos(2d_{\mathbf{n}})\sin(2d_{\mathbf{m}})$$
$$+\pi\frac{(d_{\mathbf{n}}^2-d_{\mathbf{m}}^2)^3 + 12(d_{\mathbf{n}}^2-d_{\mathbf{m}}^2)^2 - 100(d_{\mathbf{n}}^2+3d_{\mathbf{m}}^2)}{4(d_{\mathbf{n}}^2-d_{\mathbf{m}}^2)^3 d_{\mathbf{n}}}\sin(2d_{\mathbf{n}})\cos(2d_{\mathbf{m}})$$
$$+\frac{\pi}{8d_{\mathbf{n}}d_{\mathbf{m}}}\left(\frac{20}{(d_{\mathbf{n}}+d_{\mathbf{m}})^2} + \frac{20}{(d_{\mathbf{n}}-d_{\mathbf{m}})^2} + 31\right)\sin(2d_{\mathbf{n}})\sin(2d_{\mathbf{m}}). \tag{F7}$$

Here, $\gamma = 0.57722$ is the Euler-Mascheroni constant, and $\mathrm{Ci}(\bullet)$ and $\mathrm{Si}(\bullet)$ are the cosine and sine integrals, respectively.

[1] B. P. Abbott *et al.*, Phys. Rev. Lett. **116,** 061102 (2016).
[2] B. P. Abbott *et al.*, Phys. Rev. Lett. **116,** 241103 (2016).
[3] B. P. Abbott *et al.*, Phys. Rev. Lett. **118,** 221101 (2017).
[4] B. P. Abbott *et al.*, Phys. Rev. Lett. **119,** 141101 (2017).
[5] B. P. Abbott *et al.* (LIGO Scientific and Virgo Collaborations), Astrophys. J. **851,** L35 (2017).
[6] B. P. Abbott *et al.*, Phys. Rev. Lett. **119,** 161101 (2017).
[7] D. Blair *et al.*, Sci. China Phys. Mech. Astron. **58,** 120402 (2015).
[8] S. A. Hughes, S. Marka, P. L. Bender, and C. J. Hogan, eConf **C010630,** P402 (2001).
[9] B. P. Abbott *et al.* (LIGO Scientific and Virgo Collaborations), Astrophys. J. **818,** L22 (2016).
[10] A. Abbott (LIGO Scientific, VINROUGE, Las Cumbres Observatory, DES, DLT40, Virgo, 1M2H, Dark Energy Camera GW-E, and MASTER Collaborations), Nature (London) **551,** 425 (2017).
[11] B. P. Abbott *et al.*, Phys. Rev. Lett. **116,** 221101 (2016).
[12] B. P. Abbott *et al.*, Phys. Rev. X **6,** 041015 (2016).
[13] B. P. Abbott *et al.*, Astrophys. J. Lett. **848,** L13 (2017).
[14] S. Hou, Y. Gong, and Y. Liu, Eur. Phys. J. C **78,** 378 (2018).
[15] C. M. Will, Living Rev. Relativity **17,** 4 (2014).
[16] K. J. Lee, F. A. Jenet, and R. H. Price, Astrophys. J. **685,** 1304 (2008).
[17] N. J. Cornish, L. O'Beirne, S. R. Taylor, and N. Yunes, Phys. Rev. Lett. **120,** 181101 (2018).
[18] T. Prusti *et al.* (Gaia Collaboration), Astron. Astrophys. **595,** A1 (2016).
[19] G. F. Gilmore *et al.*, in *Astronomical Interferometry*, edited by R. D. Reasenberg, SPIE Proceedings Vol. 3350 (SPIE-International Society for Optical Engineering, Bellingham, WA, 1998), p. 541.
[20] V. B. Braginsky, N. S. Kardashev, A. G. Polnarev, and I. D. Novikov, Nuovo Cimento Soc. Ital. Fis. **105B,** 1141 (1990).
[21] C. R. Gwinn, T. M. Eubanks, T. Pyne, M. Birkinshaw, and D. N. Matsakis, Astrophys. J. **485,** 87 (1997).
[22] L. G. Book and E. E. Flanagan, Phys. Rev. D **83,** 024024 (2011).

[23] F. Mignard and S. Klioner, Astron. Astrophys. **547,** A59 (2012).

[24] S. A. Klioner, Classical Quantum Gravity **35,** 045005 (2018).

[25] C. J. Moore, D. P. Mihaylov, A. Lasenby, and G. Gilmore, Phys. Rev. Lett. **119,** 261102 (2017).

[26] É. É. Flanagan and S. A. Hughes, New J. Phys. **7,** 204 (2005).

[27] D. Perrodin and A. Sesana, arXiv:1709.02816.

[28] Z. Arzoumanian *et al.*, Astrophys. J. **821,** 13 (2016).

[29] L. Lentati *et al.*, Mon. Not. R. Astron. Soc. **453,** 2577 (2015).

[30] R. M. Shannon *et al.*, Science **349,** 1522 (2015).

[31] J. P. W. Verbiest *et al.*, Mon. Not. R. Astron. Soc. **458,** 1267 (2016).

[32] L. O'Beirne and N. J. Cornish, arXiv:1804.03146.

[33] J. R. Gair, J. D. Romano, and S. R. Taylor, Phys. Rev. D **92,** 102003 (2015).

[34] B. F. Schutz, IAU Symp. **261,** 234 (2010).

[35] L. S. Finn, S. L. Larson, and J. D. Romano, Phys. Rev. D **79,** 062003 (2009).

[36] A. C. Robin *et al.*, Astron. Astrophys. **543,** A100 (2012).

[37] E. E. Flanagan, Phys. Rev. D **48,** 2389 (1993).

[38] E. J. Fuselier and G. B. Wright, SIAM J. Numer. Anal. **47,** 3213 (2009).

[39] R. W. Hellings and G. S. Downs, Astrophys. J. Lett. **265,** L39 (1983).

[40] J. Gair, J. D. Romano, S. Taylor, and C. M. F. Mingarelli, Phys. Rev. D **90,** 082001 (2014).

[41] S. J. Chamberlin and X. Siemens, Phys. Rev. D **85,** 082001 (2012).